J. Fluid Mech. (2025), *vol.* 1020, A31, doi:10.1017/jfm.2025.10667

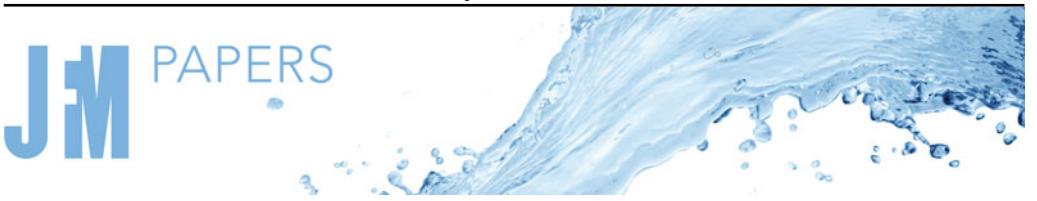

Derivation of linearly stable Onsager symmetry principle-consistent equations and their validation for force-driven Poiseuille flow

Upendra Yadav[1], **Ravi S. Jadhav**[1,2] **and Amit Agrawal**[1]

[1]Department of Mechanical Engineering, Indian Institute of Technology Bombay, Powai, Mumbai 400076, India

[2]Technology Development Advanced Modeling, Micron Technologies (Inc.), Hyderabad 500081, India

Corresponding author: Amit Agrawal, amit.agrawal@iitb.ac.in

(Received 25 October 2024; revised 24 July 2025; accepted 30 August 2025)

In this work, we derive higher-order transport equations starting from the Boltzmann equation using a second-order accurate distribution function within the 13-moment framework. The equations are shown to be unconditionally linearly stable and consistent with Onsager's symmetry principle. We also show that the equations comply with the second law of thermodynamics by establishing the non-negativity of the bulk entropy generation rate using the linearised form of the proposed equations. The force-driven Poiseuille flow problem, a standard benchmark problem, is selected to establish the validity of the equations. A complete analytical solution for this problem is proposed and compared against the Navier–Stokes, regularised 13, Grad 13 solutions and direct simulation Monte Carlo data. The proposed solution captures key rarefaction effects, including the Knudsen layer, non-uniform bimodal pressure profile, non-Fourier heat flux and the characteristic temperature dip at the centre. The analytical solution for the field variables indicates that the equations outperform the existing models in the slip- and transition-flow regimes for the problem considered. These satisfactory results point to the accuracy and applicability of the proposed equations, and the equations hold significant promise for rarefied gas dynamics at large Knudsen numbers.

Key words: Navier–Stokes equations, non-continuum effects, rarefied gas flow

1. Introduction

The field of rarefied gas dynamics deals with flows where the molecular mean free path (λ) of gas molecules is of the order of, or larger than, the characteristic length

scale (H) of the system. A critical parameter in this field is the Knudsen number ($Kn = \lambda/H$), which is used to classify different flow regimes. Of particular interest are the slip-flow ($10^{-3} < Kn < 10^{-1}$) and transition-flow ($10^{-1} < Kn < 10$) regimes, that are commonly encountered in diverse applications such as spacecraft re-entry, high-altitude flight, micro-electro-mechanical systems and advanced vacuum technologies (Cercignani 1975; Agrawal, Kushwaha & Jadhav 2020; García-Colín *et al.* 2008). Since the Navier–Stokes (N–S) equations do not yield accurate results in the slip- and transition-flow regimes, several approaches for deriving higher-order transport (HOT) equations have been proposed in the literature; their advantages and limitations are briefly covered in the ensuing paragraphs.

The development of HOT equations can be traced through three main approaches: the Chapman–Enskog approach (Chapman 1916; Enskog 1917), the moment method (Grad 1949, 1958) and the recently proposed Onsager-consistent approach (Singh & Agrawal 2016; Singh, Jadhav & Agrawal 2017; Yadav *et al.* 2023, 2024). All these approaches shun the traditional way of deriving the transport equations for a differential control volume; rather, they start from the fundamental Boltzmann kinetic equation (Struchtrup 2005; Agrawal *et al.* 2020). The Chapman–Enskog method expands the particle distribution function around the Maxwell–Boltzmann equilibrium to derive fluid-dynamic equations like the Euler, N–S, Burnett and super-Burnett equations (Burnett 1936; Shavaliyev 1993; Balakrishnan, Agarwal & Yun 1999). However, at higher orders (second and above), the Burnett and super-Burnett equations suffer from stability issues and are shown to violate the second law of thermodynamics in some cases (Bobylev 1982; Shavaliyev 1993; Uribe & Garcia 1999; García-Colín *et al.* 2008; Agrawal *et al.* 2020). To address these limitations, several variants like the augmented (Zhong, MacCormack & Chapman 1993), Bhatnagar–Gross–Krook-Burnett (Balakrishnan *et al.* 1999), regularised Burnett (Jin & Slemrod 2001) and simplified Burnett (Zhao, Chen & Agarwal 2014) equations have been proposed. These variants, however, often involve *ad hoc* modifications in the available equations as opposed to being derived from sound physical principles. For example, although the BGK-Burnett equations (Agarwal & Balakrishnan 1996; Balakrishnan 2004) were shown to yield stable, H-theorem-consistent numerical solutions, this was at the expense of assuming same relaxation times for momentum and energy, which corresponds to a non-physical unit Prandtl number (Agarwal, Yun & Balakrishnan 2001). Apart from the inherent limitations of Burnett-like equations, their most significant drawback is the challenge of deriving additional boundary conditions, as most of these equations are of third order. Despite substantial efforts since their introduction in 1936, a complete and consistent set of boundary conditions still remains unavailable.

The moment method, developed by Grad (1949, 1958), is another powerful approach that involves expanding the distribution function into a series of orthogonal Hermite polynomials. While the moment equations offer improvements over the N–S equations and can predict many rarefied flow phenomena (Reitebuch & Weiss 1999; Agrawal *et al.* 2020) they are not without limitations (Grad 1952; Weiss 1995). For example, the Grad equations form a hyperbolic set of equations that give discontinuous shocks for Mach number (Ma) > 1.65. Although we can stretch this critical Mach number limit by including more moments, the improvement is rather marginal and difficult to justify for the additional effort involved (Weiss 1995). Another drawback associated with the Gard 13 (G13) equations is the unphysical negative values of the distribution function at higher Mach numbers, as demonstrated in the planar shock wave problem (Torrilhon 2016). To mitigate some of these issues, several variants have been proposed in the literature, for example, regularised 13 (R13) (Struchtrup & Torrilhon 2003) and regularised 26 (R26) (Gu & Emerson 2009). These equations were derived using the combined Chapman–Enskog

and the Grad moment approach with an aim to bring the advantages of their underlying methods. However, the R13 equations possess an intricate structure and are generally not applicable at higher Mach and Knudsen numbers (Torrilhon 2016). Furthermore, the 26-moment equations put forth by Gu & Emerson (2009) add another layer of complexity, involving 26 independent variables and an even greater number of requisite boundary conditions. Although these equations claim to improve upon the Grad moment equations, they are inherently complex and require additional boundary conditions, thereby hindering their applicability to realistic problems.

The principle of entropy maximisation in non-equilibrium systems has a long and well-established history Kogan (1969), Dreyer (1987), Müller & Ruggeri (1993), and in recent years, the maximum entropy moment closure has gained significant attention due to its strong mathematical and physical foundations Öttinger (2010), McDonald & Torrilhon (2013), Rana & Struchtrup (2016), Rana, Gupta & Struchtrup (2018), Brini & Ruggeri (2020), Rana *et al.* (2021). A key aspect of Brini & Ruggeri (2020) is the hyperbolicity of the governing equations, which is crucial for accurately modelling the non-stationary phenomena and ensuring finite disturbance speeds. This is in contrast to parabolic models, such as the Navier–Stokes–Fourier equations, which predict infinite propagation speeds. The feasibility of using maximum entropy closure in rarefied gas simulations has been well documented; see McDonald (2011) and McDonald & Groth (2013). However, due to the high computational cost associated with this approach, precomputed values and interpolation techniques are commonly employed to improve its practicality in computational fluid dynamics McDonald & Torrilhon (2013). Furthermore, Öttinger (2005) introduced a generalised Hamiltonian structure to impose constraints on thermodynamic models, and later, Öttinger (2010) proposed modifying the 13-moment theory by redefining the heat flux variable using the pressure tensor to enforce thermodynamic admissibility. The critical review of different approaches indicates the potential to develop better closure relations, which could broaden the Knudsen number range and offer solutions extending into the mid- or late-transition regime. Any closure relation should, however, be consistent with the second law of thermodynamics. In this context, a novel approach known as the Onsager-consistent method (Singh & Agrawal 2016; Singh *et al.* 2017) has recently been proposed.

The Onsager-consistent method leverages the Onsager symmetry principle (OSP) (Onsager 1931*a*,*b*) to derive Onsager-13 moment (Grad-like) (Singh & Agrawal 2016) and Onsager–Burnett (Burnett-like) (Singh *et al.* 2017) equations. This approach can, therefore, be regarded as the third independent method to solve the Boltzmann equation and obtain HOT equations (Agrawal *et al.* 2020; Jadhav, Yadav & Agrawal 2023). Unlike the Chapman–Enskog and moment methods, the distribution function in this approach is expressed in terms of thermodynamic forces and fluxes. The resulting distribution function is not only consistent with the second law of thermodynamics but also satisfies the linearised Boltzmann equation and compatibility conditions. The Onsager–Burnett (OBurnett) equations have shown promising results when applied to problems such as force-driven Poiseuille flow (Jadhav, Singh & Agrawal 2017), Grad's second problem (Jadhav & Agrawal 2020*a*, 2021*a*), normal shock waves (Jadhav & Agrawal 2020*b*; Jadhav, Gavasane & Agrawal 2021; Jadhav & Agrawal 2021*b*) and pressure-driven Poiseuille flow (Yadav & Agrawal 2021; Jadhav *et al.* 2023). Notably, for normal shocks, the OBurnett equations produced smooth shock structures across all Mach numbers with a clear existence of heteroclinic trajectory. The equations were also shown to be consistent with the second law of thermodynamics by ensuring positive entropy generation.

Building on this above-mentioned novel approach, Yadav, Jonnalagadda & Agrawal (2023) recently derived an extended distribution function, incorporating additional terms

by substituting the material derivatives with expressions from the N–S equations. The extended-Onsager 13 (EO13) equations, derived from this distribution, have been successfully applied to isothermal Poiseuille flow and Grad's second problem (Yadav *et al.* 2023), with results showing excellent agreement with available direct simulation Monte Carlo (DSMC) data. Furthermore, the complete analytical solution for cylindrical Couette flow was obtained for the first time using the EO13 equations (Yadav & Agrawal 2024). When compared with the N–S and G13 equations, the EO13 equations demonstrated superior accuracy and quantitative agreement with DSMC data. Recently, the extended distribution function from Yadav *et al.* (2023) was further refined by adding a term through an iterative refinement technique, consistent with the Onsager-consistent approach (Yadav, Jonnalagadda & Agrawal 2024). This refined distribution function was employed to derive the extended-OBurnett and super-OBurnett equations, which were then validated for the pressure-driven Poiseuille flow.

Despite significant advances in rarefied gas dynamics, existing moment equations face notable shortcomings. Motivated by these limitations and by the recent success of the Onsager-consistent approach, we propose a more generalised set of HOT equations. This study is motivated by the following goals: (i) to ensure thermodynamic consistency of the equations via the OSP; (ii) to overcome the limitations of the existing methods, particularly their restricted validity at small Knudsen numbers; and (iii) to evaluate the predictive performance of the proposed model in comparison with established Grad moment-based formulations. The resulting set of equations should then extend the field of continuum fluid mechanics into the early and mid-transition regime and capture the non-equilibrium flow phenomena that are typically inaccessible to the N–S, G13 and conventional Burnett-type models.

The paper is organised as follows. In § 2, we summarise the generalised distribution function from Yadav *et al.* (2024). Next, in § 3, we introduce the third-order super-Onsager 13-moment (SO13) equations for Maxwellian molecules by combining the OSP with the Grad moment method, which yields the correct Prandtl number for Maxwell molecules. Section 4 examines the linear stability of the SO13 equations, while § 5 discusses their consistency with the OSP. In § 6, we demonstrate their compliance with the second law of thermodynamics. We then derive an analytical solution for force-driven Poiseuille flow in § 7 and compare it with existing models and DSMC data. Section 8 provides a comparative overview of the proposed and existing solutions, and § 9 summarises the major contributions of the present work.

2. Single-particle distribution function

The Boltzmann equation provides the kinetic theory description of the evolution of thermodynamic systems

$$\frac{\partial f}{\partial t} + \frac{\partial}{\partial \boldsymbol{x}} \cdot (\boldsymbol{c} f) = \mathscr{J}(f, f), \tag{2.1}$$

where $f = f(\boldsymbol{x}, \boldsymbol{c}, t)$ is the single-particle distribution function, $\mathscr{J}(f, f)$ is the binary collision operator and $\boldsymbol{x}$, $\boldsymbol{c}$, t are the location vector, molecular velocity and time, respectively. The solution of the Boltzmann equation (2.1) is the single-particle distribution function which serves as the connecting link between the microscopic world and the macroscopic world. Once the form of the distribution function is known on solving the Boltzmann equation, the macroscopic field variables can be obtained by taking the moments of the distribution function (Chapman & Cowling 1970; Cercignani

1975; Sone 2000; Zohar *et al.* 2002; Agrawal 2011; Agrawal *et al.* 2020). The general Onsager-consistent approach employed in the present work for evaluating an approximate form of the distribution function is discussed in detail in Mahendra & Singh (2013), Singh & Agrawal (2016), Yadav *et al.* (2023). Here, we provide only the key steps for brevity in the present section.

With the help of Chapman–Enskog expansion, the zeroth-order Maxwellian (f_0) and first-order (f_1) distribution function can be employed to derive the Euler and N–S equations, respectively. The expressions for f_0 and f_1 are given as

$$f_0(\boldsymbol{x}, \boldsymbol{c}, t) = \frac{\rho}{m}\left(\frac{\beta}{\pi}\right)^{(3/2)} \exp\left[-\beta(|\boldsymbol{c}-\boldsymbol{u}|)^2\right], \tag{2.2}$$

$$f_1(\boldsymbol{x}, \boldsymbol{c}, t) = f_0(\boldsymbol{x}, \boldsymbol{c}, t) - \underbrace{\sum_j \Upsilon_j \odot X_j,}_{\bar{f}_1}, \tag{2.3}$$

where m is the molecular mass, $\beta = 1/(2RT)$, R and $T(\boldsymbol{x}, t)$ are the specific gas constant and absolute temperature, respectively, and $\rho(\boldsymbol{x}, t)$ and $\boldsymbol{u}(\boldsymbol{x}, t)$ are the bulk density and velocity, respectively. The symbol $\odot$ denotes a full tensorial contraction for tensors of the same order. In (2.3), f_1 is obtained using the iterative refinement technique (Mahendra & Singh 2013), and is expressed in terms of thermodynamic forces X_j and the corresponding microscopic conjugate fluxes Υ_j. Here, the subscript $j = [\tau, q]$, where τ represents destabilising viscous processes and q denotes thermal non-equilibrium processes. It is important to emphasise that these formulations of X_j and Υ_j are as per the OSP.

Similar to the first-order correction term ($\bar{f}_1$) to the Maxwellian distribution function, the second-order correction term ($\bar{f}_2$) has been derived using the iterative refinement technique in Yadav *et al.* (2023, 2024) as

$$\begin{aligned} f = f_0 + \bar{f}_1 + \underbrace{(\Upsilon_{\tau\tau} \odot X_\tau) \odot X_\tau + (\Upsilon_{qq} \odot X_q) \odot X_q}_{\bar{f}_{2,1}} \\ + \underbrace{\Upsilon_\tau \odot (X_{\tau\tau} \odot X_\tau) + \Upsilon_q \odot (X_{qq} \odot X_q)}_{\bar{f}_{2,2}}, \end{aligned} \tag{2.4}$$

where the explicit expressions of $\bar{f}_{2,1}$ and $\bar{f}_{2,2}$ are documented in Yadav *et al.* (2023) and Yadav *et al.* (2024), respectively, and which depend upon either the Euler or N–S equations for substituting the material derivatives in terms of spatial derivatives. For completeness and clarity, explicit expressions are presented in Appendix A, which serves as a direct reference for the formulations discussed in this section. However, readers interested in a comprehensive derivation and its relationship with *Kn* are encouraged to refer to the works of Mahendra & Singh (2013), Singh & Agrawal (2016), Singh *et al.* (2017) and Yadav *et al.* (2023, 2024), where these aspects are thoroughly detailed.

3. Generalised set of 13-moment equations

The generalised, three-dimensional, 13-moment transport equations are obtained after evaluating the moments of the Boltzmann equation. Explicitly, this evaluation, which involves computing $\langle \Psi, (\partial f/\partial t) + (\partial/\partial \boldsymbol{x}) \cdot (\boldsymbol{c} f)\rangle = \langle \Psi, \mathscr{J}(f, f)\rangle$, where $\Psi = \{1, c_i, (C_i^2/2), C_{\langle i} C_{j\rangle}, C_i(C_k^2/2)\}$, yields the following equations (Grad 1949):

$$\frac{\partial \rho}{\partial t} + \frac{\partial \rho u_k}{\partial x_k} = 0, \tag{3.1}$$

$$\rho \frac{\partial u_i}{\partial t} + \rho u_k \frac{\partial u_i}{\partial x_k} + \frac{\partial p}{\partial x_i} + \frac{\partial \sigma_{ik}}{\partial x_k} = \rho G_i, \tag{3.2}$$

$$\rho \frac{\partial \epsilon}{\partial t} + \rho u_k \frac{\partial \epsilon}{\partial x_k} + \frac{\partial q_k}{\partial x_k} + p \frac{\partial u_k}{\partial x_k} + \sigma_{ij} \frac{\partial u_i}{\partial x_j} = 0, \tag{3.3}$$

$$\begin{aligned} &\frac{\partial \sigma_{ij}}{\partial t} + u_k \frac{\partial \sigma_{ij}}{\partial x_k} + \frac{4}{5} \frac{\partial q_{\langle i}}{\partial x_{j\rangle}} + 2\sigma_{k\langle i} \frac{\partial u_{j\rangle}}{\partial x_k} + 2p \frac{\partial u_{\langle i}}{\partial x_{j\rangle}} + \sigma_{ij} \frac{\partial u_k}{\partial x_k} \\ &\qquad + \frac{\partial}{\partial x_k} \underline{\langle C_{\langle i} C_j C_{k\rangle}, f \rangle} \langle C_{\langle i} C_{j\rangle}, \mathscr{J}(f, f) \rangle, \end{aligned} \tag{3.4}$$

$$\begin{aligned} &\frac{\partial q_i}{\partial t} + u_k \frac{\partial q_i}{\partial x_k} + \frac{5}{2} \left(\frac{p}{\rho} \frac{\partial p}{\partial x_i} - \frac{p^2}{\rho^2} \frac{\partial \rho}{\partial x_i} \right) + \frac{\partial}{\partial x_j} \frac{1}{2} \underline{\langle |C|^2 C_{\langle i} C_{j\rangle}, f \rangle} - \frac{5}{2} \frac{p}{\rho} \frac{\partial \sigma_{ik}}{\partial x_k} \\ &\quad - \frac{\sigma_{ik}}{\rho} \frac{\partial p}{\partial x_k} + \frac{1}{6} \frac{\partial}{\partial x_i} \underline{\langle |C|^4, (f - f_0) \rangle} - \frac{\sigma_{ij}}{\rho} \frac{\partial \sigma_{jk}}{\partial x_k} + \frac{7}{5} q_k \frac{\partial u_i}{\partial x_k} + \frac{7}{5} q_i \frac{\partial u_k}{\partial x_k} \\ &\quad + \frac{2}{5} q_k \frac{\partial u_k}{\partial x_i} + \frac{\partial u_j}{\partial x_k} \underline{\langle C_{\langle i} C_j C_{k\rangle}, f \rangle} = \frac{1}{2} \langle |\boldsymbol{C}|^2 C_i, \mathscr{J}(f, f) \rangle \end{aligned} \tag{3.5}$$

Here, G_i represents body force,q_i denotes the heat flux and σ_{ij} the stress tensor, and $C_{\langle i} C_j C_{k\rangle}$ is a third-order trace-free symmetric tensor, defined as (Struchtrup 2005; Agrawal *et al.* 2020)

$$w_{\langle ijk\rangle} = w_{(ijk)} - \frac{1}{5} \left(w_{(ill)} \delta_{jk} + w_{(jll)} \delta_{ik} + w_{(kll)} \delta_{ij} \right), \tag{3.6}$$

where round brackets indicate the symmetric part of a tensor. Note that only the underlined terms involving angular brackets with a comma denote moments, whereas angular brackets with indices denote traceless symmetric tensors. Here, $\epsilon = (3/2)RT$ is the specific internal energy per unit mass for a monatomic ideal gas, while $p = \rho RT$ is the thermodynamic pressure as represented by the ideal gas law. Equations (3.1)–(3.3) are the three standard hydrodynamic conservation equations. Note that the production terms in these equations, $\langle \{1, C_i, C_i^2/2\}, \mathscr{J}(f, f) \rangle$, vanish in accordance with the principles of conservation of mass, momentum and energy for particles undergoing elastic collisions. For (3.4) and (3.5), which describe the evolution of the stress tensor and heat flux vector, the production terms appear on the right-hand side. For Maxwell molecules, these production terms obtained using the BGK collision model are given as (Truesdell & Muncaster 1980)

$$\langle C_{\langle i} C_{j\rangle}, \mathscr{J}(f, f) \rangle = -\frac{p}{\mu} \sigma_{ij}, \tag{3.7}$$

$$\frac{1}{2} \langle |\boldsymbol{C}|^2 C_i, \mathscr{J}(f, f) \rangle = -\frac{2}{3} \frac{p}{\mu} q_i, \tag{3.8}$$

where σ_{ij} and q_i contain first- and second-order contributions. The dynamic viscosity and thermal conductivity are temperature-dependent functions given by $\mu(T) = \mu_0 (T/T_0)^{\varphi}$ and $\kappa(T) = \kappa_0 (T/T_0)^{\varphi}$, where μ_0 and κ_0 correspond to their values at a reference temperature T_0, and φ represents the interaction potential between gaseous molecules. The value of φ is unity for Maxwell molecules and 1/2 for hard-sphere molecules (García-Colín *et al.* 2008). Equations (3.4) and (3.5) contain three unknown underlined

higher-order moments (closure relations) that need to be computed to obtain a closed set of 13 moment equations.

3.1. *Closure relations*

To achieve closure for (3.1)–(3.5), all three underlined closure relations have been evaluated by substituting the derived distribution function (2.4) in $\langle C_{\langle i}C_jC_{k\rangle}, f\rangle$, $(1/2)\langle |C|^2C_{\langle i}C_{j\rangle}, f\rangle$ and $\langle |C|^4, (f-f_0)\rangle$, which requires integration with respect to peculiar velocity (C_i). By following Jin & Slemrod (2001) and Yadav *et al.* (2023), we, in the first step, make it more compact using the ideal gas equation, the N–S, and Fourier laws by replacing the N–S stress and heat flux terms present in the closure relations. In the second step, we neglect the fourth-order term in Knudsen number from the closure term to maintain the third-order accuracy of the governing set of SO13 equations since the remaining terms are of third-order in Knudsen number (Timokhin *et al.* 2017; Jadhav & Agrawal 2021*a*). Note that these fourth-order and third-order terms result from employing the N–S and Euler equations-based distribution function terms to evaluate the closure relations. After algebraic simplification, we obtain the following closure relationship:

$$\left\langle C_{\langle i}C_jC_{k\rangle}, f_2\right\rangle = -6\frac{pRTt^2_{r(\tau)}}{\rho}\frac{\partial\rho}{\partial x_{\langle i}}\frac{\partial u_j}{\partial x_{k\rangle}} + t_{r(\tau)}\left(-2a_sRT\frac{\partial\sigma_{\langle ij}}{\partial x_{k\rangle}} + \frac{2(8a_s-27)}{15}q_{\langle i}\frac{\partial u_j}{\partial x_{k)}}\right), \tag{3.9}$$

$$\begin{aligned}\left\langle \frac{1}{2}C_k^2C_{\langle i}C_{j\rangle}, f_2\right\rangle = {}& \frac{7}{2}\frac{p}{\rho}\sigma_{ij} + t_{r(\tau)}\left(-\frac{24a_{qv}}{5}RT\frac{\partial q_{\langle i}}{\partial x_{j\rangle}} + \frac{75}{10}\frac{1}{4}\frac{RT}{\mu}\sigma_{k\langle i}\sigma_{j\rangle k}\right.\\ & + \frac{145}{10}\frac{1}{2}RT\sigma_{k\langle i}\frac{\partial u_j}{\partial x_{k\rangle}} - \frac{1}{2}\left[\frac{49}{3} - \frac{14\varphi}{3}\right]RT\sigma_{ij}\frac{\partial u_l}{\partial x_l} + \frac{91}{15}\frac{1}{\rho}q_{\langle i}\frac{\partial p}{\partial x_{j\rangle}}\Bigg)\\ & + \frac{56-64a_{qv}}{25}\frac{1}{p}q_{\langle i}q_{j\rangle},\end{aligned} \tag{3.10}$$

$$\left\langle |C|^4, (f_2-f_0)\right\rangle = t_{r(\tau)}\left(\frac{24a_{qs}}{5}RT\frac{\partial q_k}{\partial x_k} + 12\frac{q_k}{\rho}\frac{\partial p}{\partial x_k}\right) + \frac{8\left(8a_{qs}+35\right)}{25}\frac{1}{p}q_kq_k, \tag{3.11}$$

where parameter $t_{r(\tau)}$ represents the relaxation time for momentum. Here, $a_s = 1.61$, $a_{qv} = 1/2$ and $a_{qs} = -5/2$ satisfy the compatibility condition, which represent the additive invariant property of kinetic theory (Balakrishnan *et al.* 1999; Agarwal *et al.* 2001) and are independent of the Knudsen number (Kn). For more in-depth understanding, interested readers are encouraged to refer to Balakrishnan *et al.* (1999), Yadav *et al.* (2023) and Yadav *et al.* (2024). This leads to linear stability, OSP consistency, and compliance with the second law of thermodynamics, as demonstrated later in the manuscript. Note that, despite the above-mentioned modification, while deriving the final form of the closure reactions, the accuracy level of these equations remain intact. However, the modification alters the mathematical characteristics of (3.9)–(3.11), resulting in both linear and nonlinear forms of the equations needing an equivalent number of boundary conditions. Equations (3.1)–(3.5) along with the closure relations (3.9)–(3.11) form the closed set of HOT equations being proposed in this work.

4. Linear stability analysis

In this section, we establish the one-dimensional stability of the linearised equations presented in the previous section. For this purpose, we first represent relevant quantities in

non-dimensional form as follows (Yadav *et al.* 2024):

$$\rho = \rho_o(1+\bar{\rho}),\ T = T_o(1+\bar{T}),\ p = p_o(1+\bar{p}),\ u_1 = \sqrt{RT_o}\bar{u}_1,\ \sigma_{11} = \rho_o RT_o\bar{\sigma}_{11},$$
$$q_1 = \rho_o\left(\sqrt{RT_o}\right)^3\bar{q}_1,\ x = H\bar{x},\ t = \frac{H}{\sqrt{RT_o}}\bar{t}. \tag{4.1}$$

The subscript 'o' indicates the variable at equilibrium state, the subscript '1' indicates a relevant quantity in the x-direction and H represents the characteristic length. Meanwhile, the quantities with an overbar ($\bar{\cdot}$) represent small perturbations around the equilibrium or rest state. Assuming that the perturbations are small, the analysis focuses only on linear terms, significantly simplifying the calculations. As a result, a reduced set of linearised and non-dimensionalised equations starting from (3.1)–(3.5), with closure relations given by (3.9)–(3.10), are obtained as

$$\frac{\partial\bar{\rho}}{\partial\bar{t}} + \frac{\partial\bar{u}_1}{\partial\bar{x}} = 0, \tag{4.2a}$$

$$\frac{\partial\bar{u}_1}{\partial\bar{t}} + \frac{\partial\bar{T}}{\partial\bar{x}} + \frac{\partial\bar{\rho}}{\partial\bar{x}} + \frac{\partial\bar{\sigma}_{11}}{\partial\bar{x}} = 0, \tag{4.2b}$$

$$\frac{3}{2}\frac{\partial\bar{T}}{\partial\bar{t}} + \frac{\partial\bar{q}_1}{\partial\bar{x}} + \frac{\partial\bar{u}_1}{\partial\bar{x}} = 0, \tag{4.2c}$$

$$\frac{\partial\bar{\sigma}_{11}}{\partial\bar{t}} - \frac{483}{250}Kn\frac{\partial^2\bar{\sigma}_{11}}{\partial\bar{x}^2} + \frac{8}{15}\frac{\partial\bar{q}_1}{\partial\bar{x}} + \frac{4}{3}\frac{\partial\bar{u}_1}{\partial\bar{x}} + \frac{\bar{\sigma}_{11}}{Kn} = 0, \tag{4.2d}$$

$$\frac{\partial\bar{q}_1}{\partial\bar{t}} - \frac{18}{5}Kn\frac{\partial^2\bar{q}_1}{\partial\bar{x}^2} + \frac{5}{2}\frac{\partial\bar{T}}{\partial\bar{x}} + \frac{\partial\bar{\sigma}_{11}}{\partial\bar{x}} + \frac{2\bar{q}_1}{3Kn} = 0. \tag{4.2e}$$

Now, we employ the normal mode perturbation method and assume the solution of primary variables to be of the form

$$\bar{\rho} = \rho_A\exp(\omega\bar{t} + i\kappa\bar{x}),\ \bar{u} = u_{1A}\exp(\omega\bar{t} + i\kappa\bar{x}),\ \bar{T} = T_A\exp(\omega\bar{t} + i\kappa\bar{x}),$$
$$\bar{\sigma}_{11} = \bar{\sigma}_{11A}\exp(\omega\bar{t} + i\kappa\bar{x}),\ \bar{q}_1 = \bar{q}_{1A}\exp(\omega\bar{t} + i\kappa\bar{x}). \tag{4.3}$$

Here, the variables κ, ω and the subscript 'A' represent the wavenumber, wave frequency and complex amplitude of the plane wave, respectively. By substituting these solutions (4.3) into (4.2*a*)–(4.2*e*), a relationship between κ and ω is obtained. This relationship, known as the dispersion relation, can be expressed as

$$-\frac{3\omega^5}{2} + \omega^4\left(-\frac{36\kappa^2}{5} - \frac{5}{2}\right) + \omega^3\left(-\frac{162\kappa^4}{25} - \frac{72\kappa^2}{5} - 1\right) + \omega^2\left(-\frac{111\kappa^4}{5} - 8\kappa^2\right)$$
$$+\omega\left(-\frac{54\kappa^6}{5} - \frac{31\kappa^4}{2} - \frac{5\kappa^2}{3}\right) + \left(-3\kappa^6 - \frac{5\kappa^4}{2}\right) = 0. \tag{4.4}$$

Upon obtaining (4.4), we examine the roots of this fifth-order polynomial to analyse the stability of the proposed equations. These roots, which can have both real and complex parts, provide valuable insights into the system's behaviour when subjected to disturbances in space. As a result, we consider a real wavenumber and complex frequency represented by $\omega = \omega_r(\kappa) + i\omega_i(\kappa)$.

In order to ensure stability, it is essential to satisfy the condition $\omega_r(\kappa) = Re(\omega) \leqslant 0$, indicating that the real part, $Re(\omega)$, of the frequency is negative. This ensures that the local amplitude of primary variables decreases over time in the presence of spatial disturbances. The stability analysis is reinforced by the solutions obtained from (4.4), which yield five roots for ω. These roots are shown in figure 1(*a*), clearly illustrating the stability criterion.

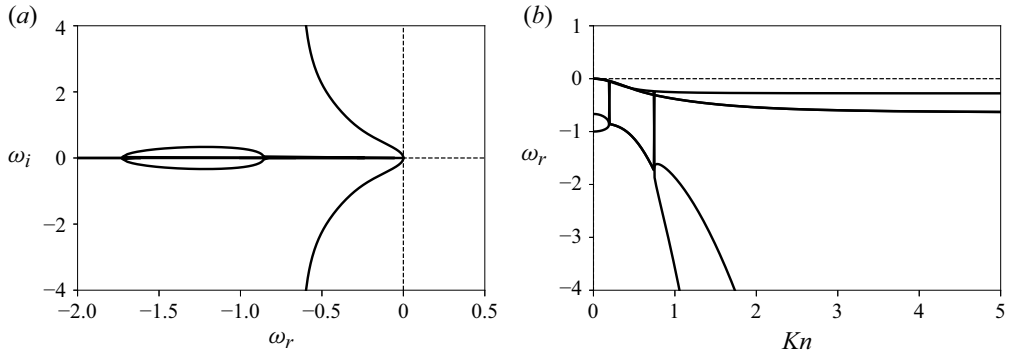

Figure 1. (*a*) Stability curve of the SO13 equations due to spatial perturbations. (*b*) Variation of attenuation coefficient with Knudsen number.

Further, variation of the attenuation coefficient ($\omega_r(\kappa)$) has been shown in figure 1(*b*), in which $Kn\,(=\mu_o\sqrt{RT_o}/(p_oH))\approx\kappa$ is adopted for convenience, as demonstrated in Balakrishnan *et al.* (1999). This assumption serves as an approximate representation of the validity and stability range of the proposed equations. It is important to note that the absence of this assumption does not affect the generality of the stability analysis of the present equations. Figure 1(*b*) shows that all five roots are negative for any value of the Knudsen number. Thus, the proposed SO13 moment equations are unconditionally stable for small spatial disturbances and are therefore free from the Bobylev instability, a well-known issue that plagues the Burnett and other HOT equations.

5. Compliance with Onsager symmetry principle

Here, we follow the procedure outlined by Romero & Velasco (1995) and express the perturbed field variables ($\hat{\rho}, \hat{u}_i, \hat{\epsilon}, \hat{\sigma}_{ij}, \hat{q}_i$) in terms of thermodynamic forces in the corresponding hydrodynamic fields ($X_\rho, X_{u,i}, X_\epsilon, X_{\sigma_{ij}}, X_{q_i}$). The linearisation is performed about a local equilibrium state using the following perturbation structure: $\rho=\rho_o+\hat{\rho}, \quad T=T_o+\hat{T}, \quad p=p_o+\hat{p}, \quad u_i=\hat{u}_i, \quad \sigma_{ij}=\hat{\sigma}_{ij}, \quad q_i=\hat{q}_i$, where the subscript o denotes equilibrium values and variables with a hat ($\hat{}$) represent small deviations around the equilibrium state. Explicitly, these forces are given as (Singh & Agrawal 2016)

$$X_\rho=\frac{1}{\rho_oT_o}\hat{p}-\frac{p_o}{\rho_o}X_\epsilon,\ X_{u_i}=\frac{1}{T_o}\hat{u}_i,\ X_\epsilon=\frac{1}{T_o^2}\hat{T},\ X_{\sigma_{ij}}=\frac{1}{2p_oT_o}\hat{\sigma}_{ij},\ X_{q_i}=\frac{2}{5p_oRT_o^2}\hat{q}_i. \tag{5.1}$$

We further substitute the perturbed field variables and the closure relations given by (3.9)–(3.10) in (3.1)–(3.5). Note that the ideal gas law is explicitly employed to express the pressure in terms of density. The governing equations are then linearised after substitution, which results in the following simplified SO13 equations containing both first- and second-order derivative terms:

$$\frac{\partial\hat{\rho}}{\partial t}=-\rho_o\frac{\partial\hat{u}_k}{\partial x_k}, \tag{5.2}$$

$$\rho_o\frac{\partial\hat{u}_i}{\partial t}=-\frac{\partial\hat{p}}{\partial x_i}-\frac{\partial\hat{\sigma}_{ik}}{\partial x_k}, \tag{5.3}$$

$$\rho_o \frac{\partial \hat{\epsilon}}{\partial t} = -\frac{\partial \hat{q}_k}{\partial x_k} - p_o \frac{\partial \hat{u}_k}{\partial x_k}, \tag{5.4}$$

$$\frac{\partial \hat{\sigma}_{ij}}{\partial t} = \frac{161}{100} \frac{RT_o \mu_o}{p_o} \frac{\partial}{\partial x_k} \frac{\partial \hat{\sigma}_{\langle ij}}{\partial x_{k\rangle}} - \frac{4}{5} \frac{\partial \hat{q}_{\langle i}}{\partial x_{j\rangle}} - 2p_o \frac{\partial \hat{u}_{\langle i}}{\partial x_{j\rangle}} - \frac{p_o}{\mu_o} \hat{\sigma}_{ij}, \tag{5.5}$$

$$\frac{\partial \hat{q}_i}{\partial t} = \frac{1}{2} \frac{RT_o \mu_o}{p_o} \frac{\partial}{\partial x_j} \frac{\partial \hat{q}_{\langle i}}{\partial x_{j\rangle}} - \frac{5}{12} \frac{RT_o \mu_o}{p_o} \frac{\partial^2 \hat{q}_k}{\partial x_i \partial x_k} - \frac{5}{2} Rp_o \frac{\partial \hat{T}}{\partial x_i} - \frac{p_o}{\rho_o} \frac{\partial \hat{\sigma}_{ik}}{\partial x_k} - \frac{2}{3} \frac{p_o}{\mu_o} \hat{q}_i, \tag{5.6}$$

where μ_o denotes equilibrium values. Finally, (5.1) is used to replace the perturbed quantities present in the linearised moment equations (5.2)–(5.6), which yields

$$\frac{\partial \hat{\rho}}{\partial t} = -T_o \rho_o \frac{\partial X_{u_i}}{\partial x_i}, \tag{5.7}$$

$$\frac{\partial \hat{u}_i}{\partial t} = -T_o p_o \frac{\partial X_\epsilon}{\partial x_i} - 2T_o p_o \frac{\partial X_{\sigma_{ij}}}{\partial x_j} - T_o \rho_o \frac{\partial X_\rho}{\partial x_i}, \tag{5.8}$$

$$\frac{\partial \hat{\epsilon}}{\partial t} = -\frac{5RT_o^2 p_o}{2} \frac{\partial X_{q_i}}{\partial x_i} - T_o p_o \frac{\partial X_{u_i}}{\partial x_i}, \tag{5.9}$$

$$\frac{\partial \hat{\sigma}_{ij}}{\partial t} = \frac{161}{50} RT_o \mu_o \frac{\partial}{\partial x_k} \frac{\partial X_{\sigma\langle ij}}{\partial x_{k\rangle}} - 2RT_o^2 p_o \frac{\partial X_{q\langle i}}{\partial x_{j\rangle}} - \frac{2T_o p_o^2}{\mu_o} X_{\sigma_{ij}} - 2T_o p_o \frac{\partial X_{u\langle i}}{\partial x_{j\rangle}}, \tag{5.10}$$

$$\frac{\partial \hat{q}_i}{\partial t} = \frac{5}{24} R^2 T_o^2 \mu_o \frac{\partial^2 X_{q\langle i}}{\partial x_j \partial x_{j\rangle}} - \frac{5RT_o^2 p_o^2}{3\mu_o} X_{q_i} - \frac{5RT_o^2 p_o}{2} \frac{\partial X_\epsilon}{\partial x_i} - 2RT_o^2 p_o \frac{\partial X_{\sigma_{ik}}}{\partial x_k}. \tag{5.11}$$

Further, (5.7)–(5.11) can be recast into a compact form as

$$\frac{\partial \alpha_i}{\partial t} = -\sum_j L_{ij} X_j, \tag{5.12}$$

where X_j is provided in (5.1), and α_i represents all the primary variables present in the proposed equations and the matrix of phenomenological coefficients, L_{ij}, is given as

$$L_{ij} = \begin{bmatrix} 0 & -T_o \rho_o \nabla & 0 & 0 & 0 \\ -T_o \rho_o \nabla & 0 & -T_o p_o \nabla & -2T_o p_o \nabla & 0 \\ 0 & -T_o p_o \nabla & 0 & 0 & -\frac{5RT_o^2 p_o \nabla}{2} \\ 0 & -2T_o p_o \nabla & 0 & \frac{161 RT_o \mu_o \nabla^2}{50} - \frac{2T_o p_o^2}{\mu_o} & -2RT_o^2 p_o \nabla \\ 0 & 0 & -\frac{5RT_o^2 p_o \nabla}{2} & -2RT_o^2 p_o \nabla & \frac{5R^2 T_o^2 \mu_o \nabla^2}{24} - \frac{5RT_o^2 p_o^2}{3\mu_o} \end{bmatrix}. \tag{5.13}$$

Here, ∇ denotes the first-order spatial derivative operator (i.e. $\partial/\partial x_i$), and ∇^2 represents the Laplacian operator. It is important to note that the matrix L_{ij} does not contain any terms involving the operator $(\partial^2/\partial x_i \partial x_k)$.

A system of equations of the form of (5.12) is compliant with the OSP if the Hermitian conjugate of the matrix of phenomenological coefficients, $L^\dagger$, satisfies the relation $L^\dagger = DLD$ (McLennan 1974; Romero & Velasco 1995). Here, D is a diagonal matrix with elements $D_{ii} = \mp 1$ based on the odd/even parity of the primary variables under time reversal.

For (5.7)–(5.11), D is explicitly evaluated to be

$$D = \begin{bmatrix} 1 & 0 & 0 & 0 & 0 \\ 0 & -1 & 0 & 0 & 0 \\ 0 & 0 & 1 & 0 & 0 \\ 0 & 0 & 0 & 1 & 0 \\ 0 & 0 & 0 & 0 & -1 \end{bmatrix}. \tag{5.14}$$

For matrix L given in (5.13), $L^{\dagger}$ is given as

$$\begin{bmatrix} 0 & T_o\rho_o\nabla & 0 & 0 & 0 \\ T_o\rho_o\nabla & 0 & T_o p_o\nabla & 2T_o p_o\nabla & 0 \\ 0 & T_o p_o\nabla & 0 & 0 & \frac{5RT_o^2 p_o\nabla}{2} \\ 0 & 2T_o p_o\nabla & 0 & \frac{161RT_o\mu_o\nabla^2}{50} - \frac{2T_o p_o^2}{\mu_o} & 2RT_o^2 p_o\nabla \\ 0 & 0 & \frac{5RT_o^2 p_o\nabla}{2} & 2RT_o^2 p_o\nabla & \frac{5R^2T_o^2\mu_o\nabla^2}{24} - \frac{5RT_o^2 p_o^2}{3\mu_o} \end{bmatrix}, \tag{5.15}$$

which can be trivially shown to satisfy $L^{\dagger} = DLD$, thus proving that (5.7)–(5.11) satisfy the OSP. Most available HOT equations do not satisfy the OSP, and thus, the compliance of the proposed model with the OSP highlights a significant theoretical contribution.

6. Compliance with second law of thermodynamics

From Struchtrup & Torrilhon (2007), the bulk entropy generation rate for the Grad moment-based transport equations for the Maxwellian molecule is presented as

$$\Sigma_b = \frac{1}{2Kn}\sigma_{ij}\sigma_{ij} + \frac{2}{5}\frac{Pr}{Kn}q_i q_i - \frac{1}{2}A_{ijk}\frac{\partial\sigma_{ij}}{\partial x_k} - \frac{9}{20}Pr^2 B_{ik}\frac{\partial q_i}{\partial x_k}, \tag{6.1}$$

where subscript b in Σ_b denotes the bulk variation of the entropy generation rate and Pr is the Prandtl number. Here, the last two terms arise from the additional terms in the closure expression compared with the G13 equations. Note that the tensors A_{ijk} and B_{ik} represent only the linear terms in the closure expression. As a result, from (3.9)–(3.11), the expression of A_{ijk} and B_{ij} are given as

$$A_{ijk} = -2Kna_s\frac{\partial\sigma_{\langle ij}}{\partial x_{k\rangle}}, \quad B_{ij} = -\frac{24}{5}a_{qv}Kn\frac{\partial q_{\langle i}}{\partial x_{j\rangle}} + \frac{8}{5}Kna_{qs}\frac{\partial q_k}{\partial x_k}\delta_{ij}, \tag{6.2}$$

where only linear terms are considered for simplicity and tensor A_{ijk} represents the linear terms from 3.9, while B_{ij} corresponds to the sum of the linear terms from (3.10)–(3.11). Here, the coefficients a_α ($\alpha \in \{s, qv, qs\}$) are already defined in § 3, where the first two coefficients are positive while the last one is negative. For the Maxwell molecule, these coefficients were obtained naturally from kinetic theory while following the compatibility conditions. Unlike our closure, the standard Grad closure does not include terms associated with a_α ($\alpha \in \{s, qv, qs\}$), effectively neglecting certain dissipative effects. Hence, setting $a_\alpha = 0$ in our closure equations does not directly recover the Grad 13-moment closure due to the presence of additional nonlinear terms.

Here, Σ_b must remain non-negative, $\Sigma_b \geqslant 0$, for all variables such as $\rho, u_i, T, \sigma_{ij}, q_i$. This condition can be readily shown by substituting (6.2) in (6.1) and then by performing algebraic operations. Consequently, we obtain the following simplified expression for Σ_b as:

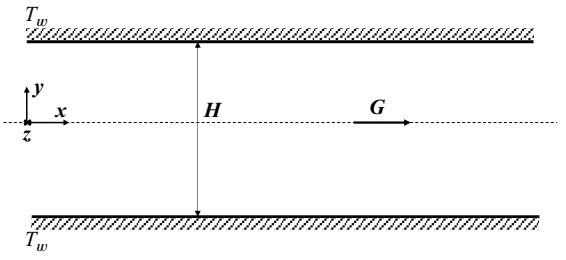

Figure 2. The diagram shows the compressible plane Poiseuille flow problem, driven by an external force (G). The upper and lower plate temperatures are assumed to have the same temperature T_w.

$$\Sigma_b = \frac{1}{2Kn}\sigma_{ij}\sigma_{ij} + \frac{2}{5}\frac{Pr}{Kn}q_i q_i + 1.61\,Kn\frac{\partial\sigma_{\langle ij}}{\partial x_{k\rangle}}\frac{\partial\sigma_{ij}}{\partial x_k} + \frac{9}{20}Pr^2 Kn\left(\frac{12}{5}\frac{\partial q_{\langle i}}{\partial x_{j\rangle}} + 4\frac{\partial q_k}{\partial x_k}\delta_{ij}\right)\frac{\partial q_i}{\partial x_j}. \tag{6.3}$$

It is important to observe that cross-coupling terms are absent in (6.3) owing to the restriction of (6.1) to the linearised form of the governing equations, as documented in Struchtrup & Torrilhon (2007). Since the last two terms of (6.3) appear with the same sign but with different coefficients, as in the case of the R13 equations presented in Struchtrup & Torrilhon (2007), this ensures that Σ_b remains positive under all conditions.

7. Poiseuille flow

This section aims to analytically solve the two-dimensional compressible plane Poiseuille flow problem driven by a streamwise external force (G) by employing the semi-linearisation method (Yadav *et al.* 2023; Yadav & Agrawal 2024). Despite its simplicity, planar Poiseuille flow serves as an ideal test case for validating the proposed equations due to its distinct non-equilibrium behaviours. Extensive studies have shown that, under dilute conditions, these flows exhibit phenomena beyond the predictive scope of the Navier–Stokes–Fourier framework, including a flow-aligned heat flux without a temperature gradient (Uribe & Garcia 1999; Aoki, Takata & Nakanishi 2002), a non-uniform pressure profile (Tij & Santos 1994; Aoki *et al.* 2002) and a characteristic temperature depression (Aoki *et al.* 2002; Zheng, Garcia & Alder 2002; Xu 2003). This will be followed by comparing our analytical solution with different existing models and DSMC simulation data to validate the analytical solution.

7.1. *Analytical solution for Poiseuille flow*

The schematic of the force-driven plane Poiseuille flow problem is presented in figure 2, which has two parallel plates separated by a distance H, and the origin is located at the centre of the channel's entrance. The flow is driven by a body force (shown as 'G' in the figure). To derive the solution for this problem, we simplify the problem depicted in figure 2 by assuming that the flow remains steady and that all primary variables depend only on the normal direction of the flow. In this analysis, we further assume that the viscosity (μ) remains constant and independent of the temperature. Additionally, it should be noted that the cross-stream velocity (v) is zero due to the presence of impermeable bounding walls. By employing the assumptions mentioned above and simplifications for this flow problem, we finally obtain the following variables:

$$u_i = \begin{bmatrix} u_1(y) \\ 0 \\ 0 \end{bmatrix}, \ \sigma_{ij} = \begin{bmatrix} \sigma_{11}(y) & \sigma_{12}(y) & 0 \\ \sigma_{12}(y) & \sigma_{22}(y) & 0 \\ 0 & 0 & -\sigma_{11}(y) - \sigma_{22}(y) \end{bmatrix}, \ q_i = \begin{bmatrix} q_1(y) \\ q_2(y) \\ 0 \end{bmatrix}. \tag{7.1}$$

We introduce a set of dimensionless variables in (7.2), which allows further simplification of (3.1)–(3.5)

$$\bar{y} = \frac{y}{H}, \quad \bar{\rho} = \frac{\rho - \rho_o}{\rho_o}, \quad \bar{T} = \frac{T - T_o}{T_o}, \quad \bar{G} = \frac{H}{RT_o}G, \quad \bar{u}_1 = \frac{u_1}{\sqrt{RT_o}}, \quad \bar{\sigma}_{ij} = \frac{\sigma_{ij}}{\rho_o RT_o},$$
$$\bar{q}_1 = \frac{q_1}{\rho_o \sqrt{RT_o}^3}. \tag{7.2}$$

The substitution of (7.2) in (3.1)–(3.5) and considering the assumptions for the present analysis, we obtain

$$x\text{-Momentum equation}: -\bar{G} + \frac{\mathrm{d}\bar{\sigma}_{12}}{\mathrm{d}\bar{y}} = 0, \tag{7.3a}$$

$$y\text{-Momentum equation}: \frac{\mathrm{d}\bar{T}}{\mathrm{d}\bar{y}} + \frac{\mathrm{d}\bar{\rho}}{\mathrm{d}\bar{y}} + \frac{\mathrm{d}\bar{\sigma}_{22}}{\mathrm{d}\bar{y}} = 0, \tag{7.3b}$$

$$\text{Energy equation}: \bar{\sigma}_{12}\frac{\mathrm{d}\bar{u}_1}{\mathrm{d}\bar{y}} + \frac{\mathrm{d}\bar{q}_2}{\mathrm{d}\bar{y}} = 0, \tag{7.4}$$

$$\text{Stress equation for } \bar{\sigma}_{11}: \frac{1412Kn^2}{1875}\frac{\mathrm{d}\bar{\sigma}_{12}}{\mathrm{d}\bar{y}}\frac{\mathrm{d}^2\bar{u}_1}{\mathrm{d}\bar{y}^2} - \frac{161Kn}{150}\frac{\mathrm{d}^2\bar{\sigma}_{11}}{\mathrm{d}\bar{y}^2} + \frac{161Kn}{375}\frac{\mathrm{d}^2\bar{\sigma}_{22}}{\mathrm{d}\bar{y}^2} + \frac{4}{3}\bar{\sigma}_{12}\frac{\mathrm{d}\bar{u}_1}{\mathrm{d}\bar{y}} - \frac{4}{15}\frac{\mathrm{d}\bar{q}_2}{\mathrm{d}\bar{y}} + \frac{1}{Kn}\bar{\sigma}_{11} = 0, \tag{7.5a}$$

$$\text{Stress equation for } \bar{\sigma}_{12}: -\frac{644Kn}{375}\frac{\mathrm{d}^2\bar{\sigma}_{12}}{\mathrm{d}\bar{y}^2} + \frac{2}{5}\frac{\mathrm{d}\bar{q}_1}{\mathrm{d}\bar{y}} + \frac{\mathrm{d}\bar{u}_1}{\mathrm{d}\bar{y}} + \frac{1}{Kn}\bar{\sigma}_{12} = 0, \tag{7.5b}$$

$$\text{Stress equation for } \bar{\sigma}_{22}: -\frac{353Kn^2}{625}\frac{\mathrm{d}\bar{\sigma}_{12}}{\mathrm{d}\bar{y}}\frac{\mathrm{d}^2\bar{u}_1}{\mathrm{d}\bar{y}^2} - \frac{483Kn}{250}\frac{\mathrm{d}^2\bar{\sigma}_{22}}{\mathrm{d}\bar{y}^2} - \frac{2}{3}\bar{\sigma}_{12}\frac{\mathrm{d}\bar{u}_1}{\mathrm{d}\bar{y}} + \frac{8}{15}\frac{\mathrm{d}\bar{q}_2}{\mathrm{d}\bar{y}} + \frac{1}{Kn}\bar{\sigma}_{22} = 0, \tag{7.5c}$$

$$\text{Heat flux equation for } \bar{q}_1: -\frac{6}{5}Kn\frac{\mathrm{d}^2\bar{q}_1}{\mathrm{d}\bar{y}^2} + \frac{1}{2}\frac{\mathrm{d}\bar{\sigma}_{12}}{\mathrm{d}\bar{y}} + \frac{1}{3Kn}\bar{q}_1 = 0, \tag{7.6a}$$

$$\text{Heat flux equation for } \bar{q}_2: -\frac{29Kn}{12}\bar{\sigma}_{12}\frac{\mathrm{d}^2\bar{u}_1}{\mathrm{d}\bar{y}^2} - \frac{18Kn}{5}\frac{\mathrm{d}^2\bar{q}_2}{\mathrm{d}\bar{y}^2} - \frac{2067Kn}{500}\frac{\mathrm{d}\bar{\sigma}_{12}}{\mathrm{d}\bar{y}}\frac{\mathrm{d}\bar{u}_1}{\mathrm{d}\bar{y}} + \frac{2}{5}\bar{q}_1\frac{\mathrm{d}\bar{u}_1}{\mathrm{d}\bar{y}} + \frac{1}{4}\bar{\sigma}_{12}\frac{\mathrm{d}\bar{\sigma}_{12}}{\mathrm{d}\bar{y}} + \frac{5}{2}\frac{\mathrm{d}\bar{T}}{\mathrm{d}\bar{y}} + \frac{\mathrm{d}\bar{\sigma}_{22}}{\mathrm{d}\bar{y}} + \frac{2}{3Kn}\bar{q}_2 = 0. \tag{7.6b}$$

The above set of equations is expressed in terms of the Knudsen number ($Kn = \mu_0\sqrt{RT_0}/(p_0H)$), which characterises the degree of rarefaction. Note that the Knudsen number is determined based on the equilibrium state ρ_0, T_0. In (7.3*a*)–(7.6*b*), linear terms are retained along with key nonlinear contributions. Following Yadav *et al.* (2023), the equations include nonlinear viscous heating terms, $\bar{\sigma}_{21}(\mathrm{d}\bar{u}_1/\mathrm{d}\bar{y})$ and $\bar{q}_1(\mathrm{d}\bar{u}_1/\mathrm{d}\bar{y})$, as well as their combinations, which appear in the SO13 equation and higher-order closure relations. These terms account for key phenomena, including viscous heating

and non-hydrodynamic effects. Specifically, the first term in (7.6*b*), which is first-order in Knudsen number, arises from this consideration.

Integration of (7.3*a*) results in

$$\bar{\sigma}_{21} = \bar{G}\bar{y} + C_{\sigma_{21}}, \tag{7.7}$$

where $C_{\sigma_{21}}$ represents an integration constant (appropriate subscripts have been added to the constants to indicate their origin). Subsequently, by solving the coupled equations (7.6*a*) and (7.5*b*) while incorporating (7.7), we obtain the following simultaneous solution:

$$\bar{q}_1 = C_{q_{11}} \sinh(A) + C_{q_{12}} \cosh(A) - \frac{3\bar{G}Kn}{2}, \tag{7.8}$$

$$\bar{u}_1 = C_{u_1} - \frac{C_{\sigma_{21}}}{Kn}\bar{y} - \frac{2C_{q_{11}}}{5}\sinh(A) - \frac{2C_{q_{12}}}{5}\cosh(A) + \frac{3\bar{G}Kn}{5} - \frac{\bar{G}}{2Kn}\bar{y}^2, \tag{7.9}$$

where $A = (\sqrt{5}\bar{y}/3Kn)$, the integration constants are represented by $C_{q_{11}}$, $C_{q_{12}}$ and C_{u_1}. Upon incorporating (7.7)–(7.9) into (7.4), we obtain the subsequent expression

$$\begin{aligned}\bar{q}_2 = {} & C_{q_{21}} + \frac{2C_{q_{11}}C_{\sigma_{21}}}{5}\sinh(A) - \frac{6\sqrt{5}C_{q_{11}}\bar{G}Kn}{25}\cosh(A) + \frac{2C_{q_{11}}\bar{G}\bar{y}}{5}\sinh(A) \\ & + \frac{2C_{q_{12}}C_{\sigma_{21}}}{5}\cosh(A) - \frac{6\sqrt{5}C_{q_{12}}\bar{G}Kn}{25}\sinh(A) + \frac{2C_{q_{12}}\bar{G}\bar{y}}{5}\cosh(A) + \frac{C_{\sigma_{21}}^2}{Kn}\bar{y} \\ & + \frac{C_{\sigma_{21}}\bar{G}}{Kn}\bar{y}^2 + \frac{\bar{G}^2}{3Kn}\bar{y}^3,\end{aligned} \tag{7.10}$$

where $C_{q_{21}}$ is an integration constant. Thereafter, integrating (7.5*a*) and (7.5*c*) individually yields the solution for the normal stresses ($\bar{\sigma}_{11}$, and $\bar{\sigma}_{22}$) as follows:

$$\begin{aligned}\bar{\sigma}_{11} = {} & C_{\sigma_{111}} \sinh(C) + C_{\sigma_{112}} \cosh(C) + \frac{8C_{\sigma_{21}}^2}{5} \\ & - \frac{912\sqrt{5}C_{q_{11}}C_{\sigma_{21}}}{1199}\cosh(A) + \frac{10580600056C_{q_{11}}\bar{G}Kn}{107820075}\sinh(A) \\ & - \frac{912\sqrt{5}C_{q_{11}}\bar{G}}{1199}\bar{y}\cosh(A) - \frac{912\sqrt{5}C_{q_{12}}C_{\sigma_{21}}}{1199}\sinh(A) \\ & + \frac{10580600056C_{q_{12}}\bar{G}Kn}{107820075}\cosh(A) - \frac{912\sqrt{5}C_{q_{12}}\bar{G}}{1199}\bar{y}\sinh(A) \\ & + \frac{16C_{\sigma_{21}}\bar{G}}{5}\bar{y} - \frac{C_{\sigma_{221}}}{2}\sinh(B) - \frac{C_{\sigma_{222}}}{2}\cosh(B) + \frac{9784\bar{G}^2Kn^2}{1875} + \frac{8\bar{G}^2}{5}\bar{y}^2,\end{aligned} \tag{7.11a}$$

$$\begin{aligned}\bar{\sigma}_{22} = {} & C_{\sigma_{221}} \sinh(B) + C_{\sigma_{222}} \cosh(B) - \frac{3251\bar{G}^2Kn^2}{625} + \frac{24\sqrt{5}C_{q_{11}}C_{\sigma_{21}}}{11}\cosh(A) \\ & - \frac{1723268C_{q_{11}}\bar{G}Kn}{9075}\sinh(A) + \frac{24\sqrt{5}C_{q_{11}}\bar{G}}{11}\bar{y}\cosh(A) + \frac{24\sqrt{5}C_{q_{12}}C_{\sigma_{21}}}{11}\sinh(A) \\ & - \frac{1723268C_{q_{12}}\bar{G}Kn}{9075}\cosh(A) + \frac{24\sqrt{5}C_{q_{12}}\bar{G}}{11}\bar{y}\sinh(A) - \frac{6C_{\sigma_{21}}^2}{5} - \frac{12C_{\sigma_{21}}\bar{G}}{5}\bar{y} \\ & - \frac{6\bar{G}^2}{5}\bar{y}^2,\end{aligned} \tag{7.11b}$$

where $B = (5\sqrt{4830}\bar{y}/483Kn)$, $C = (5\sqrt{966}\bar{y}/161Kn)$, while $C_{\sigma_{111}}$, $C_{\sigma_{112}}$, $C_{\sigma_{221}}$ and $C_{\sigma_{222}}$ are integration constants. Finally, thermodynamic variables (T, and p) are obtained after integrating (7.6*b*) and (7.3*b*) individually as

$$\begin{aligned}\bar{T} = {} & C_T + \frac{4C_{q_{11}}^2}{125}\cosh^2(A) + \frac{8C_{q_{11}}C_{q_{12}}}{125}\sinh(A)\cosh(A) - \frac{9623\sqrt{5}C_{q_{11}}C_{\sigma_{21}}}{12375}\cosh(A) \\ & + \frac{85851704C_{q_{11}}\bar{G}Kn}{1134375}\sinh(A) - \frac{9623\sqrt{5}C_{q_{11}}\bar{G}}{12375}\bar{y}\cosh(A) + \frac{4C_{q_{12}}^2}{125}\cosh^2(A) \\ & - \frac{9623\sqrt{5}C_{q_{12}}C_{\sigma_{21}}}{12375}\sinh(A) + \frac{85851704C_{q_{12}}\bar{G}Kn}{1134375}\cosh(A) - \frac{9623\sqrt{5}C_{q_{12}}\bar{G}}{12375}\bar{y}\sinh(A) \\ & - \frac{2C_{\sigma_{21}}^2}{15Kn^2}\bar{y}^2 + \frac{3299C_{\sigma_{21}}\bar{G}}{3750}\bar{y} - \frac{4C_{\sigma_{21}}\bar{G}}{45Kn^2}\bar{y}^3 - \frac{2C_{\sigma_{221}}}{5}\sinh(B) - \frac{2C_{\sigma_{222}}}{5}\cosh(B) \\ & - \frac{4C_{q21}}{15Kn}\bar{y} + \frac{3299\bar{G}^2}{7500}\bar{y}^2 - \frac{\bar{G}^2}{45Kn^2}\bar{y}^4, \end{aligned} \tag{7.12a}$$

$$\begin{aligned}\bar{p} = {} & C_p - \frac{24\sqrt{5}C_{q_{11}}C_{\sigma_{21}}}{11}\cosh(A) + \frac{1723268C_{q_{11}}\bar{G}Kn}{9075}\sinh(A) - \frac{24\sqrt{5}C_{q_{11}}\bar{G}}{11}\bar{y}\cosh(A) \\ & - \frac{24\sqrt{5}C_{q_{12}}C_{\sigma_{21}}}{11}\sinh(A) + \frac{1723268C_{q_{12}}\bar{G}Kn}{9075}\cosh(A) - \frac{24\sqrt{5}C_{q_{12}}\bar{G}}{11}\bar{y}\sinh(A) \\ & + \frac{6C_{\sigma_{21}}^2}{5} + \frac{12C_{\sigma_{21}}\bar{G}}{5}\bar{y} - C_{\sigma_{221}}\sinh(B) - C_{\sigma_{222}}\cosh(B) + \frac{3251\bar{G}^2Kn^2}{625} + \frac{6\bar{G}^2}{5}\bar{y}^2, \end{aligned} \tag{7.12b}$$

where C_T and C_p are integration constants.

It is important to highlight that the N–S equations predict zero streamwise heat flux, while the G13 equations predict a constant streamwise heat flux. Note that the velocity ($\bar{u}_1$), heat flux ($\bar{q}_1$, $\bar{q}_2$) and shear stress component ($\bar{\sigma}_{21}$) explicitly depend on the forcing term ($\bar{G}$), whereas other physical quantities ($\bar{T}$, $\bar{p}$) and the normal stress components ($\bar{\sigma}_{11}$, $\bar{\sigma}_{22}$) become non-zero due to their coupling with the previously mentioned parameters.

Note that the expression for density ($\bar{\rho}$) is derived from pressure and temperature, as it is a dependent variable. Hence, it is not presented here for brevity. Within this context, it is crucial to note that the integration constants $C_{\sigma_{21}}$, $C_{q_{11}}$, $C_{\sigma_{221}}$ and $C_{q_{21}}$, which are present in (7.7)–(7.10), become zero due to the symmetry displayed by the streamwise velocity and temperature. Incorporating these results into (7.10)–(7.12*b*) results in the following analytical solution of various quantities for the problem:

$$\bar{\sigma}_{21} = \underline{\bar{G}\bar{y}}, \tag{7.13a}$$

$$\bar{q}_1 = C_{q_{12}}\cosh(A) - \frac{3\bar{G}Kn}{2}, \tag{7.13b}$$

$$\bar{u}_1 = \underline{C_{u_1} - \frac{\bar{G}\bar{y}^2}{2Kn}} - \frac{2C_{q_{12}}}{5}\cosh(A) + \frac{3\bar{G}Kn}{5}, \tag{7.13c}$$

$$\bar{q}_2 = -\frac{6\sqrt{5}C_{q_{12}}\bar{G}Kn}{25}\sinh(A) + \frac{2C_{q_{12}}\bar{G}}{5}\bar{y}\cosh(A) + \underline{\frac{\bar{G}^2}{3Kn}\bar{y}^3}, \tag{7.13d}$$

$$\bar{\sigma}_{11} = C_{\sigma_{111}}\sinh(C) + C_{\sigma_{112}}\cosh(C) - \frac{C_{\sigma_{221}}}{2}\sinh(B) - \frac{912\sqrt{5}C_{q_{12}}\bar{G}}{1199}\bar{y}\sinh(A)$$

$$+\frac{10580600056C_{q_{12}}\bar{G}Kn}{107820075}\cosh(A)-\frac{C_{\sigma_{222}}}{2}\cosh(B)+\frac{9784\bar{G}^2Kn^2}{1875}+\frac{8\bar{G}^2}{5}\bar{y}^2, \tag{7.13e}$$

$$\bar{\sigma}_{22}=-\frac{1723268C_{q_{12}}\bar{G}Kn}{9075}\cosh(A)+\frac{24\sqrt{5}C_{q_{12}}\bar{G}}{11}\bar{y}\sinh(A)$$
$$+C_{\sigma_{221}}\sinh(B)+C_{\sigma_{222}}\cosh(B)-\frac{3251\bar{G}^2Kn^2}{625}-\frac{6\bar{G}^2}{5}\bar{y}^2, \tag{7.13f}$$

$$\bar{T}=\underline{C_T-\frac{\bar{G}^2}{45Kn^2}\bar{y}^4}+\frac{3299\bar{G}^2}{7500}\bar{y}^2+\frac{4C_{q_{12}}^2}{125}\cosh^2(A)+\frac{85851704C_{q_{12}}\bar{G}Kn}{1134375}\cosh(A)$$
$$-\frac{9623\sqrt{5}C_{q_{12}}\bar{G}}{12375}\bar{y}\sinh(A)-\frac{4C_{q21}}{15Kn}\bar{y}-\frac{2C_{\sigma_{221}}}{5}\sinh(B)-\frac{2C_{\sigma_{222}}}{5}\cosh(B), \tag{7.13g}$$

$$\bar{p}=\underline{Cp}+\frac{1723268C_{q_{12}}\bar{G}Kn}{9075}\cosh(A)-\frac{24\sqrt{5}C_{q_{12}}\bar{G}}{11}\bar{y}\sinh(A)-C_{\sigma_{221}}\sinh(B)$$
$$-C_{\sigma_{222}}\cosh(B)+\frac{3251\bar{G}^2Kn^2}{625}+\frac{6\bar{G}^2}{5}\bar{y}^2. \tag{7.13h}$$

The underlined terms in (7.13) represent the specific components that arise from the solution derived by employing the N–S equations for the present problem. We also compare our solution with that of the G13 equations in § 8. All the other terms, including the hyperbolic cosine and sine, are the result of the Knudsen layer responsible for rarefaction effects. The solutions obtained for the force-driven plane Poiseuille flow problem in (7.13) will be compared and validated against other model solutions and DSMC data in the subsequent subsection.

7.2. *Validation*

In this subsection, we compare the solution obtained from the simplified form of SO13 equations (7.13) with the N–S, G13, R13 equations and DSMC data reported in Zheng *et al.* (2002, 2003). This comparison requires evaluating the integration constants in the solution using accurate boundary conditions, which are crucial for determining these constants. However, note that extended models beyond the Navier–Stokes–Fourier framework require additional boundary conditions: the Burnett equations necessitate higher-order gradients, while Grad-type methods involve prescribing conditions for higher-order moments. Since ill-posed boundary conditions can lead to unphysical results, their careful formulation is essential. However, deriving precise boundary conditions remains an active research area for most HOT equations. It should be noted that deriving boundary conditions for the proposed equations is beyond the scope of this work. While we plan to address this issue in future work, as done in Rana & Struchtrup (2016) and Rana *et al.* (2021), we choose to proceed without being hindered by the lack of boundary conditions. Therefore, we adopt the approach suggested in Uribe & Garcia (1999), García-Colín *et al.* (2008), Yadav & Agrawal (2024) and Yadav *et al.* (2024). Accordingly, we use data from DSMC simulations to evaluate the integration constants and thereby obtain a complete solution for all the variables.

In the simplified solution of (7.13), five integration constants require five boundary conditions for the corresponding variables at one wall, as listed in table 1, while symmetry determines those at the other. It implies that the integration constants are evaluated by matching the analytical solutions with DSMC data at the wall. Note that in classical

Variables	N–S	G13	R13	SO13
$C_{q_{12}}$	0	0	3.94×10^{-4}	3.94×10^{-4}
C_{u_1}	0.577	0.577	0.580	0.580
$C_{\sigma_{222}}$	0	0	6.03×10^{-5}	1.37×10^{-3}
C_T	1.047	1.040	1.038	1.044
C_p	1.047	1.033	1.037	1.037

Table 1. Integration coefficients for various models based on DSMC data at the wall.

hydrodynamics, where Knudsen boundary layers are absent, integration constants linked to it vanish.

As discussed above, we utilise the DSMC data reported in Zheng *et al.* (2002, 2003) to evaluate the boundary conditions at $\bar{y} = \pm 0.5$ for all the primary variables. In a similar manner, we also apply this step to every result presented in the current work for other equations, namely, the N–S, G13 and R13 equations, to make the comparisons on a common ground. Note that the DSMC simulation was conducted for a non-dimensional force of $\bar{G} = 0.2355$ and a Knudsen number of $Kn = 0.072$, with the Knudsen number adjusted to match the definition used in the present study. In addition to these non-dimensional parameters, the boundary values of the primary variables obtained from the DSMC data are employed to evaluate the integration constants and their values are summarised in table 1. These values are subsequently used to obtain their profiles across the channel in the following section.

Figure 3 presents a comprehensive comparison of the results from the derived analytical solution of the proposed SO13, other (N–S, G13, R13) equations and DSMC data for the problem considered under the above-mentioned conditions. As discussed above, the remaining integration constants ($C_{q_{12}}$ and C_{u_1}), which arise after applying the symmetry conditions in (7.7)–(7.13*d*), are evaluated using the available DSMC data.

Figure 3(*a*) focuses on the variation of shear stress ($\bar{\sigma}_{21}$), which exhibits a linear profile. Notably, the profiles derived from the SO13 and other equations are indistinguishable and show good agreement with the DSMC data. Similarly, the streamwise heat fluxes ($\bar{q}_1$) obtained from the SO13 and R13 equations overlap (figure 3*b*) and align well with the DSMC data, in which the profile transitions from negative in the bulk region to positive near the wall boundaries. The change in sign indicates that the tangential heat flux is in the opposite direction to the flow direction in the bulk region. Also, we observe steep variation near the walls while the heat flux remains constant in the bulk region. The solution of the N–S equations gives zero tangential heat flux, while the G13 equations yield a constant value, which matches the solution of the SO13 equations at the centre of the microchannel. For streamwise velocity ($\bar{u}_1$) and cross-stream heat flux ($\bar{q}_2$), as shown in figures 3(*c*) and 3(*d*), respectively, the results of all equations set are indistinguishable and consistent with the DSMC data.

In figure 4, we compare the analytical solutions for normal stress ($\bar{\sigma}_{22}$), pressure ($\bar{p}$), temperature ($\bar{T}$) and density ($\bar{\rho}$) as obtained using the SO13 equations with those of the N–S, G13, R13 equations and benchmark with the DSMC data. The variation of $\bar{\sigma}_{22}$ across the microchannel (figure 4*a*) is better captured with the SO13 equations as compared with the N–S, G13 and R13 solutions. In particular, the N–S equations essentially give zero stresses, while the G13 equations fail to capture the bi-modal profile. The non-uniform pressure profile across the microchannel is accurately captured with the SO13 equations (figure 4*b*), with the N–S equations predicting a constant pressure profile.

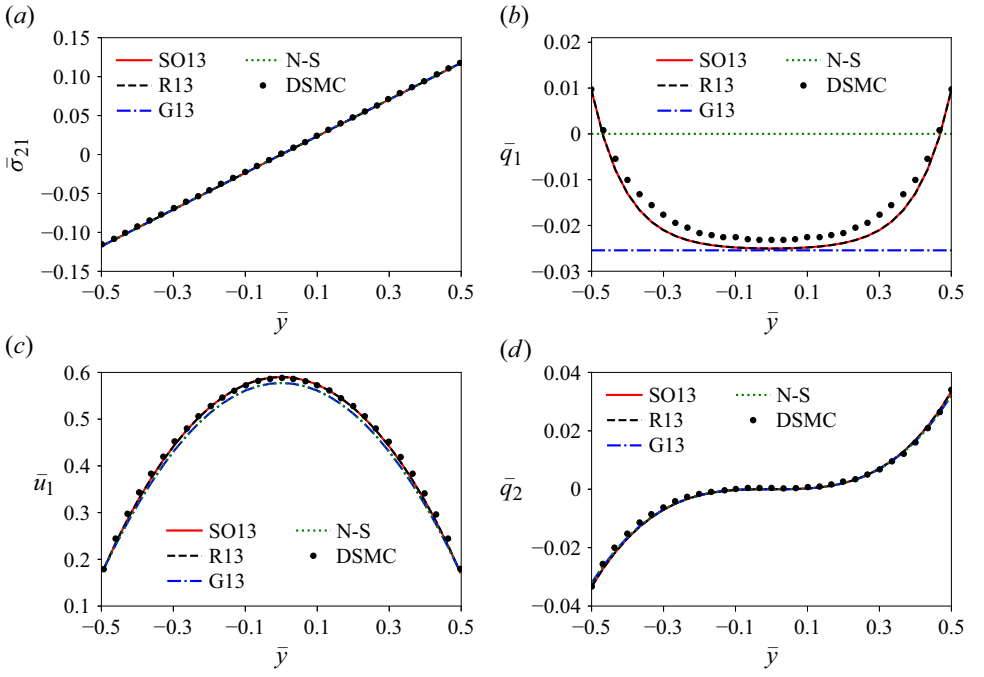

Figure 3. Cross-stream variation of (*a*) shear stress ($\bar{\sigma}_{21}$), (*b*) streamwise heat flux ($\bar{q}_1$), (*c*) streamwise velocity ($\bar{u}_1$) and (*d*) cross-stream heat flux ($\bar{q}_2$). The solution is compared with the corresponding results from the N–S, G13 and R13 equations and the DSMC data (reported by Zheng *et al.* 2002, 2003) for $Kn = 0.072$ and $\bar{G} = 0.2355$.

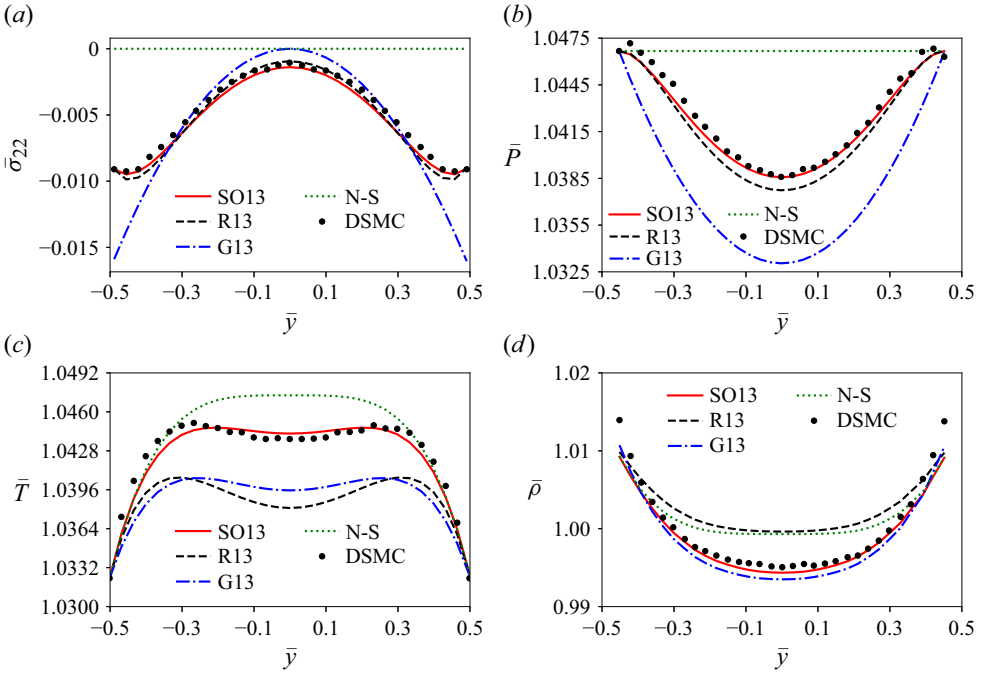

Figure 4. Cross-stream variation of (*a*) normal stress ($\bar{\sigma}_{22}$), (*b*) pressure ($\bar{p}$), (*c*) temperature ($\bar{T}$) and (*d*) density (ρ). The solution is also compared with the corresponding results from the N–S, G13 and R13 equations and the DSMC data (reported by Zheng *et al.* 2002, 2003) for $Kn = 0.072$ and $\bar{G} = 0.2355$.

The results for temperature are particularly interesting, with the DSMC simulations showing a characteristic temperature dip at the centre. As shown in figure 4(*c*), the N–S equations fail to capture this dip while the results of the SO13 equations are in better agreement with the DSMC data as compared with those of the G13 and R13 equations. Figure 4(*d*) compares the normalised density across the channel height. The results of the SO13 equations match closely with the DSMC data, thereby again establishing the superiority of the SO13 equations.

8. Discussion

In this section, we aim to touch upon the three important aspects: (i) comparison of the SO13 equations with the existing equations, (ii) provide new insights by pointing out the significance and novelty of the present work and (iii) the rigorous verification of the proposed theory with previous analytical and simulation results.

8.1. *Comparison with the N–S, G13 and R13 equations*

In this paper, we utilise the second-order OSP-consistent distribution function (Yadav *et al.* 2024) to derive closure relations for the Grad moment-based SO13 equations. Unlike the G13 equations (Grad 1949), these closure relations (3.9)–(3.11) for the SO13 incorporate several additional linear and nonlinear third-order terms in Knudsen number. As a result, the proposed SO13 equations align with the super-Burnett equations. Moreover, as compared with the N–S and G13 equations, these additional terms ensure the wider applicability of the SO13 equations in terms of Knudsen number. We compare the present closure relationships (8.1)–(8.3) with the corresponding ones from the G13 and R13 equations. Specifically, only the first term on the right-hand side of (8.2) is identical to the corresponding closure in the G13 equations. Similarly, all terms in (8.1), except the first, all terms in (8.2), except the fifth and seventh, and all terms in (8.3), except the last, are present in the R13 equation variant presented in Struchtrup (2004). Apart from this, stability issue of the equations is a well-known challenge when working with HOT equations, primarily due to the inclusion of additional linear terms (Struchtrup 2004). Therefore, building on the works of Singh & Agrawal (2016) and Yadav *et al.* (2023), we assessed the linear stability of the SO13 equations in spatial domains. The findings affirm that the proposed equations are linearly stable, a critical characteristic needed for their successful numerical implementation. The additional terms in the Burnett equations may be a source of inconsistency with the second law of thermodynamics (García-Colín *et al.* 2008). However, in the proposed SO13 theory, the additional terms does not violate the second law of thermodynamics, as demonstrated in § 6. It is important to note that, while the choice of Maxwellian molecules simplifies the derivation (particularly the collision integrals appearing in the transport equations for stress tensor and heat flux vector), the framework can be adapted to more realistic intermolecular potentials, such as Lennard–Jones or *ab initio*, by modifying the transport coefficients (Torrilhon & Struchtrup 2004). Future work will focus on extending this approach to enhance its applicability to real gas behaviours

$$\left\langle C_{\langle i}C_jC_{k\rangle},\, f_2\right\rangle = \frac{-6\dfrac{pRTt_{r(\tau)}^2}{\rho}\dfrac{\partial\rho}{\partial x_{\langle i}}\dfrac{\partial u_j}{\partial x_{k\rangle}}}{+\,t_{r(\tau)}\left(-2a_sRT\dfrac{\partial\sigma_{\langle ij}}{\partial x_{k\rangle}}+\dfrac{2(8a_s-27)}{15}q_{\langle i}\dfrac{\partial u_j}{\partial x_{k\rangle}}\right)}, \tag{8.1}$$

$$\left\langle \frac{1}{2}C_k^2 C_{\langle i}C_{j\rangle},\, f_2 \right\rangle = \frac{7}{2}\frac{p}{\rho}\sigma_{ij} + t_{r(\tau)}\left(-\frac{24a_{qv}}{5}RT\frac{\partial q_{\langle i}}{\partial x_{j\rangle}} + \frac{75}{10}\frac{1}{4}\frac{RT}{\mu}\sigma_{k\langle i}\sigma_{j\rangle k} + \frac{145}{10}\frac{1}{2}RT\sigma_{k\langle i}\frac{\partial u_j}{\partial x_{k\rangle}} - \underline{\frac{1}{2}\left[\frac{49}{3} - \frac{14\varphi}{3}\right]RT\sigma_{ij}\frac{\partial u_l}{\partial x_l}} + \frac{91}{15}\frac{1}{\rho}q_{\langle i}\frac{\partial p}{\partial x_{j\rangle}}\right) + \underline{\frac{56 - 64a_{qv}}{25}\frac{1}{p}q_{\langle i}q_{j\rangle}}, \tag{8.2}$$

$$\left\langle |C|^4,\, (f_2 - f_0)\right\rangle = t_{r(\tau)}\left(\frac{24a_{qs}}{5}RT\frac{\partial q_k}{\partial x_k} + 12\frac{q_k}{\rho}\frac{\partial p}{\partial x_k}\right) + \underline{\frac{8(8a_{qs} + 35)}{25}\frac{1}{p}q_k q_k}. \tag{8.3}$$

8.2. *Significance, novelty and advantages of the present work*

The closure of the N–S and G13 equations consists solely of linear terms, which are sufficient to capture the rarefied flow dynamics within the equilibrium regime. However, to accurately model the flow phenomena away from equilibrium, additional nonlinear terms are necessary. These terms are essential for capturing the non-equilibrium processes in rarefied flows, particularly the Knudsen layer near boundaries, which the N–S and G13 equations cannot effectively represent. With the inclusion of these additional terms (3.9)–(3.11), the SO13 equations extend the capabilities of the G13 equations, offering greater accuracy in capturing the rarefied phenomena and with a broader applicability over a wider range of Knudsen numbers. This claim is supported by the SO13 equations capability in capturing non-uniform pressure profile (Uribe & Garcia 1999; Zheng *et al.* 2002; Rana *et al.* 2016), the temperature dip at the flow centre (Tibbs, Baras & Garcia 1997; Uribe & Garcia 1999; Aoki *et al.* 2002; Xu 2003; Taheri, Torrilhon & Struchtrup 2009; Myong 2011) and the presence of a tangential heat flux without a temperature gradient (Mansour, Baras & Garcia 1997; Todd & Evans 1997; Uribe & Garcia 1999; Zheng *et al.* 2002, 2003; Taheri *et al.* 2009; Myong 2011), as shown in the present work.

Previously, the consistency of the OSP was tested for the Burnett equations (McLennan 1974; Romero & Velasco 1995) and more recently for the Onsager-13-moment equation (Singh & Agrawal 2016). McLennan (1974) and Romero & Velasco (1995) identified that the inclusion of higher-order (third-order) linear derivative terms leads to OSP violations in the Burnett equations due to initial slip. In contrast, the G13 equations contain only first-order linear derivative terms, and as a result, previous studies did not consider second-order linear derivatives when analysing OSP consistency for G13-like equations. In this work, however, we demonstrate that our proposed equations are fully compliant with the OSP, even when second-order linear derivative terms are included. This is established by proving $L^\dagger = DLD$ in (5.15). Unlike earlier approaches, we impose no restrictions on the order of the derivatives when selecting the linear terms, allowing these terms to appear as diagonal elements in the matrix. This approach is essential for testing the limits of OSP, which is typically applied to second-order differential operators, thus making our work novel in its methodology. In addition, we demonstrate that the linear form of the proposed equations is consistent with the second law of thermodynamics. This consistency provides some indication that the analysis could be relevant beyond the specific case examined here, although further studies would be needed to assess its broader applicability.

As shown in table 2, the analytical solution for the G13 equations has been derived using the semi-linear method. As a result, the temperature expression for the G13 equations contains additional terms compared with the N–S equations. Consequently, the G13 equations are capable of qualitatively capturing the third-order temperature dip effect at the centre of the microchannel, a phenomenon not previously reported in the literature, to the best of

Variable	G13 equations	N–S equations	SO13 equations	R13 equations
$\bar{q}_1$	$-\frac{3\bar{G}Kn}{2}$	0	(7.13*b*)	Equation (35) (Taheri *et al.* 2009)
$\bar{u}_1$	$C_{u_1}+\frac{3\bar{G}Kn}{5}-\frac{\bar{G}\bar{y}^2}{2Kn}$	$C_{u_1}-\frac{\bar{G}\bar{y}^2}{2Kn}$	(7.13*c*)	Equation (35) (Taheri *et al.* 2009)
$\bar{q}_2$	$\frac{\bar{G}^2\bar{y}^3}{3Kn}$	$\frac{\bar{G}^2\bar{y}^3}{3Kn}$	(7.13*d*)	Equation (36) (Taheri *et al.* 2009)
$\bar{\sigma}_{22}$	$-\frac{6\bar{G}^2\bar{y}^2}{5}$	0	(7.13*f*)	Equation (36) (Taheri *et al.* 2009)
$\bar{T}$	$C_T+\frac{14\bar{G}^2\bar{y}^2}{25}-\frac{\bar{G}^2\bar{y}^4}{45Kn^2}$	$C_T-\frac{\bar{G}^2\bar{y}^4}{45Kn^2}$	(7.13*g*)	Equation (36) (Taheri *et al.* 2009)
$\bar{p}$	$C_p+\frac{6\bar{G}^2\bar{y}^2}{5}$	C_p	(7.13*h*)	No explicit expression for p is given in Taheri*et al.* (2009); p is obtained using T and σ_{22}.

Table 2. Comparison of primary variable solutions derived from the G13, N–S, R13 and SO13 equations.

the authors' knowledge. This result suggests that the temperature dip effect at the centre may also be a nonlinear phenomenon. Furthermore, the solution and behaviour of the G13 equations have not been reported in the literature previously (Uribe & Garcia 1999; Xu 2003). Table 2 demonstrates that $\bar{q}_2$ is only a first-order effect, while $\bar{q}_1$ and $\bar{\sigma}_{11}$ are second-order effects and lie beyond the scope of the N–S equations. In this context, first-order and second-order effects correspond to the first and second powers of Knudsen number. Furthermore, a comparison of the solutions for $\bar{T}$ reveals that the N–S equations predict a local maximum, whereas the G13 equations predict a local minimum at the centre of the channel. This local minimum is also observed in the DSMC data and is accurately captured by the proposed SO13 equations. Apart from this, the results presented in figures 3 and 4 show that the accuracy of the SO13 equations is better than the available equations. Therefore, this comparison signifies the consistency of OSP and the second law of thermodynamics and enhances our faith in its applicability at a higher Knudsen number.

The inclusion of additional linear and nonlinear terms involving q_i enables the SO13 equations to be applied to phonon hydrodynamics (Guyer & Krumhansl 1966; Guo, Jou & Wang 2016), which is crucial for thermal management in the semiconductor industry. This novel approach unifies rarefied gas dynamics and phonon hydrodynamics, suggesting that a single set of equations can serve both these applications. A key advantage of this method is that, unlike other phonon hydrodynamics models, it does not rely on any free parameters. The additional nonlinear terms ($q_{\langle i}q_{j\rangle}$ and q_kq_k) are expected to play a significant role in heat conduction at small scales, where large temperature gradients are particularly important, especially in semiconductor applications.

8.3. *Comparison and validation of analytical solution*

To validate the SO13 equations, we analytically solve the force-driven Poiseuille flow using the semi-linearisation method, as applied in Yadav *et al.* (2023), Yadav & Agrawal (2024). This method accounts for several nonlinear terms in the SO13 equations compared with the G13 and N–S equations, as shown in table 2. While the solution for $\bar{q}_2$ remains identical in N–S and G13 equations, differences in $\bar{u}_1$ and $\bar{T}$ arise due to additional terms in G13, which are crucial for capturing Knudsen layer effects near boundaries.

A key observation is that the analytical solutions of the SO13 and R13 equations coincide for $\bar{\sigma}_{21}$, $\bar{q}_1$, $\bar{q}_2$ and $\bar{u}_1$ (figures 3*a* and 4*d*). As a result, their plots overlap and show an excellent agreement with DSMC data, outperforming the N–S and G13 equations. However, significant discrepancies appear in figures 4(*a*)–4(*d*), where the

N–S equations predict zero $\bar{\sigma}_{22}$ and constant pressure, while the G13 equations fail to provide qualitative accuracy. From figure 4(*b*), we would like to emphasise that the same DSMC data have been used to determine the boundary conditions for the N–S, G13, R13 and SO13 equations. Despite this, the N–S, G13 and R13 equations fail to accurately capture the pressure variation near the wall, whereas the SO13 equations more accurately align with the DSMC results. This suggests that the improved accuracy of the SO13 equations is due to their inherent higher-order modelling rather than a mere dependence on the boundary conditions. Moreover, as shown in figure 4(*c*), the N–S solution does not capture the temperature dip at the channel centre, a third-order effect previously reported in Uribe & Garcia (1999), Xu (2003). Interestingly, despite being second-order accurate, the G13 equations qualitatively capture this dip, outperforming the R13 equations at the centre. However, capturing the temperature profile accurately requires the additional hyperbolic terms in the SO13 equations, significantly differentiating their performance from G13, as demonstrated in figure 4(*c*). The discrepancies in figure 4(*d*) primarily stem from the constant pressure assumption in the N–S and under-predicted temperature in the R13 equations. Previous studies (Uribe & Garcia 1999) highlighted the challenges in capturing pressure curvature near walls using the conventional Burnett equations without DSMC fine tuning. In contrast, the SO13 solutions naturally follow the pressure variation, reinforcing confidence in their application to rarefied gas problems.

The SO13 equations are found to be the most accurate when compared with the N–S, G13 and R13 equations. It is important to note that the variation of $\bar{\rho}$ in the case of the N–S equations is not constant, even though the pressure remains constant, due to the non-uniform nature of the temperature across the channel. Some discrepancies between our analytical results and DSMC data may be due to the assumption of constant viscosity in our approach, which excludes temperature-dependent nonlinear effects. The assumption of constant viscosity, adopted for analytical simplicity as in Taheri *et al.* (2009), is justified by the minimal temperature variation in this study, with figure 4(*c*) showing approximately 1 % for $((T_{max} - T_{min})/T_{max}) \times 100$.

In summary, the present study advances the field of continuum fluid mechanics by developing the SO13 equations, a higher-order moment-based transport model that systematically bridges the kinetic theory and continuum formulations through thermodynamically consistent corrections. In the case of force-driven Poiseuille flow, the SO13 equations demonstrate improved accuracy in capturing several non-equilibrium features as compared with the existing continuum models. Notably, while the G13 equations surprisingly capture the central temperature dip qualitatively despite being second-order, the SO13 model offers quantitatively superior predictions in line with DSMC data. Furthermore, the SO13 framework is likely to provide a unified and parameter-free basis to describe both the rarefied gas dynamics and phonon-mediated thermal transport in semiconductors.

9. Conclusions

In this study, we derived generalised third-order SO13 equations for rarefied gas dynamics, which are linearly stable, consistent with the OSP and with the second law of thermodynamics. These equations incorporate additional higher-order linear and nonlinear terms, which are not present in the G13 equations. This enables our equations to accurately capture non-equilibrium phenomena such as the Knudsen layer. To validate the model, we analytically solved the force-driven Poiseuille flow problem and compared the results with DSMC data for both conserved and non-conserved variables. We evaluated the performance of the derived equations against the G13 equations, as well as the reported

solutions of the N–S and R13 equations. Our results show that, surprisingly, the second-order G13 equations qualitatively capture the temperature dip at the microchannel centre, a third-order effect well known in the literature. However, the results of the proposed SO13 equations indicate that they perform better compared with other theories in capturing critical rarefied phenomena qualitatively and quantitatively, including a non-uniform pressure profile, the central temperature dip and a tangential heat flux. The consistency of the SO13 equations with the second law of thermodynamics, along with their improved performance in the present benchmark case, suggests their potential applicability to a broader class of rarefied gas dynamics problems. However, further benchmark tests are needed in order to fully establish the validity and accuracy of the proposed equations, which we intend to present in future work.

Funding. U.Y. acknowledges the funding received through the IPDF scheme from IIT Bombay. A.A. gratefully acknowledges SERB for the JC Bose National Fellowship. These financial grants were crucial for undertaking this study.

Declaration of interests. The authors report no conflict of interest.

Appendix A. Expansion of single-particle distribution

Simplifying (2.3) yields (Yadav *et al.* 2024)

$$\Upsilon_i = -f_0\, t_{r(i)}\, \bar{\Upsilon}_i\,, \tag{A1a}$$

where

$$\bar{\Upsilon}_\tau = -\left[\boldsymbol{C}\otimes\boldsymbol{C} - \frac{1}{3}|\boldsymbol{C}|^2\boldsymbol{\delta}\right], \tag{A1b}$$

$$\bar{\Upsilon}_q = -\left(\frac{5}{2\beta} - |\boldsymbol{C}|^2\right)\boldsymbol{C}, \tag{A1c}$$

and

$$X_\tau = \beta[\boldsymbol{\nabla}\otimes\boldsymbol{u} + (\boldsymbol{\nabla}\otimes\boldsymbol{u})^T], \tag{A1d}$$

$$X_q = \boldsymbol{\nabla}\beta. \tag{A1e}$$

The quantity $\boldsymbol{\delta}$ and symbol $\otimes$ denote the Kronecker delta and the outer product, respectively. The peculiar velocity is defined as $\boldsymbol{C} = (\boldsymbol{c} - \boldsymbol{u})$. We highlight the use of distinct relaxation times for momentum ($t_{r(\tau)} = \mu/p$) and energy transport ($t_{r(q)} = \kappa(\gamma - 1)/(R\gamma p) = t_{r(\tau)}/Pr$), which not only separate viscous and thermal time scales but also ensure the correct Prandtl number Pr for gases. The quantities γ and p in $t_{r(q)}$ denote the adiabatic index and thermodynamic pressure, respectively.

In the above paragraph, the relationship between relaxation time and transport properties is provided based on Struchtrup & Torrilhon (2003) and Singh & Agrawal (2016). Furthermore, the dependence of viscosity on the Knudsen number is discussed in § 4. Together, these relations support the interpretation that higher-order corrections (first and second orders) in relaxation time correspond to an expansion in the Knudsen number, thereby systematically capturing rarefaction effects.

In (2.4), the terms $\Upsilon_{\tau\tau} \odot X_\tau$ and $\Upsilon_{qq} \odot X_q$ are, respectively, defined as (Yadav *et al.* 2024)

$$\Upsilon_{\tau\tau} \odot \boldsymbol{X}_\tau = t_{r(\tau)}^2 f_0 \left\{ \begin{array}{l} \underbrace{-C_l \left[C_i \dfrac{\partial u_j}{\partial x_l} + \left(C_j \dfrac{\partial u_i}{\partial x_l} \right)^T \right]}_{\omega_1} + \underbrace{\dfrac{1}{2\beta} \left[C_i \dfrac{\partial g}{\partial x_j} + \left(C_j \dfrac{\partial g}{\partial x_i} \right)^T \right]}_{\omega_2} \\ - \left[\underbrace{\dfrac{1}{3\beta} C_k \dfrac{\partial g}{\partial x_k}}_{\omega_3} - \underbrace{\dfrac{1}{3\beta} (\boldsymbol{C} \otimes \boldsymbol{C}) : X_\tau}_{\omega_4} \right] \delta_{ij} + \bar{\Upsilon}_\tau \left[\underbrace{\bar{\Upsilon}_\tau : X_\tau}_{\omega_5} + \underbrace{\bar{\Upsilon}_q \cdot X_q}_{\omega_6} \right] \\ + \bar{\Upsilon}_\tau \left[\underbrace{\dfrac{2\varphi - 5}{3} \dfrac{\partial u_l}{\partial x_l}}_{\omega_7} + \underbrace{\dfrac{\varphi}{\beta} C_l \dfrac{\partial \beta}{\partial x_l}}_{\omega_8} + \underbrace{C_l \dfrac{\partial g}{\partial x_l}}_{\omega_9} \right] \end{array} \right\}, \tag{A2a}$$

and

$$\Upsilon_{qq} \odot X_q = t_{r(q)}^2 f_o \left\{ \begin{array}{l} \underbrace{\bar{\Upsilon}_q \left[\bar{\Upsilon}_\tau : X_\tau + \bar{\Upsilon}_q \cdot X_q \right]}_{\xi_1} - C_i \left[\underbrace{\dfrac{1}{\beta} C_l \dfrac{\partial g}{\partial x_l}}_{\xi_2} - \underbrace{\dfrac{1}{\beta} (\boldsymbol{C} \otimes \boldsymbol{C}) : X_\tau}_{\xi_3} \right] \\ - C_i \left[\underbrace{\dfrac{5}{3\beta} \dfrac{\partial u_k}{\partial x_k}}_{\xi_4} + \underbrace{\dfrac{5}{2\beta^2} C_l \dfrac{\partial \beta}{\partial x_l}}_{\xi_5} \right] + \left(\dfrac{5}{2\beta} - |C|^2 \right) \left[\underbrace{\dfrac{1}{2\beta} \dfrac{\partial g}{\partial x_i}}_{\xi_6} - \underbrace{C_l \dfrac{\partial u_i}{\partial x_l}}_{\xi_7} \right] \\ + \bar{\Upsilon}_q \left[\underbrace{\dfrac{2\varphi - 5}{3} \dfrac{\partial u_l}{\partial x_l}}_{\xi_8} + \underbrace{\dfrac{\varphi}{\beta} C_l \dfrac{\partial \beta}{\partial x_l}}_{\xi_9} + \underbrace{C_l \dfrac{\partial g}{\partial x_l}}_{\xi_{10}} \right] \end{array} \right\}, \tag{A2b}$$

where $g = \ln(\rho/\beta)$. The remaining terms, $X_{\tau\tau} \odot X_\tau$ and $X_{qq} \odot X_q$, in the same equation are defined as follows (Yadav *et al.* 2024):

$$\begin{aligned} X_{\tau\tau} \odot X_\tau = t_{r(\tau)} \Bigg(& \underbrace{\left[\frac{1}{\beta} \frac{\partial \beta}{\partial x_j} \frac{\partial g}{\partial x_i} - \frac{\partial}{\partial x_j} \frac{\partial g}{\partial x_i} \right]}_{\omega_{10}} - 2\beta \underbrace{\frac{\partial u_i}{\partial x_k} \frac{\partial u_k}{\partial x_j}}_{\omega_{11}} + \underbrace{\frac{4}{3} \beta \frac{\partial u_l}{\partial x_l} \frac{\partial u_i}{\partial x_j}}_{\omega_{12}} \\ & + C_l \underbrace{\left[2\beta \frac{\partial}{\partial x_l} \frac{\partial u_i}{\partial x_j} + 2 \frac{\partial \beta}{\partial x_l} \frac{\partial u_i}{\partial x_j} \right]}_{\omega_{13}} \Bigg), \end{aligned} \tag{A3}$$

and

$$X_{qq} \odot X_q = t_{r(q)} \left(\underbrace{\frac{2}{3}\left[\frac{\partial \beta}{\partial x_i}\frac{\partial u_l}{\partial x_l} + \beta \frac{\partial}{\partial x_i}\frac{\partial u_l}{\partial x_l}\right]}_{\xi_{11}} - \underbrace{\frac{\partial \beta}{\partial x_k}\frac{\partial u_k}{\partial x_i}}_{\xi_{12}} + \underbrace{C_l\left[\frac{\partial}{\partial x_l}\frac{\partial \beta}{\partial x_i}\right]}_{\xi_{13}} \right). \tag{A4}$$

References

Agarwal, R.K. & Balakrishnan, R. 1996 Numerical simulation of BGK-Burnett equations. Tech. Rep. WICHITA STATE UNIV KS.

Agarwal, R.K., Yun, K.-Y. & Balakrishnan, R. 2001 Beyond Navier–Stokes: Burnett equations for flows in the continuum–transition regime. *Phys. Fluids* **13** (10), 3061–3085.

Agrawal, A. 2011 A comprehensive review on gas flow in microchannels. *Intl J. Micro-Nano Scale Transp.* **2** (1), 1–40.

Agrawal, A., Kushwaha, H.M. & Jadhav, R.S. 2020 *Microscale Flow and Heat Transfer: Mathematical Modelling and Flow Physics*. Springer.

Aoki, K., Takata, S. & Nakanishi, T. 2002 Poiseuille-type flow of a rarefied gas between two parallel plates driven by a uniform external force. *Phys. Rev. E* **65** (2), 026315.

Balakrishnan, R. 2004 An approach to entropy consistency in second-order hydrodynamic equations. *J. Fluid Mech.* **503**, 201–245.

Balakrishnan, R., Agarwal, R.K. & Yun, K.-Y. 1999 BGK-Burnett equations for flows in the continuum-transition regime. *J. Thermophys. Heat Transfer* **13** (4), 397–410.

Bobylev, A.V. 1982 The Chapman–Enskog and Grad methods for solving the Boltzmann equation. In *Akademiia Nauk SSSR Doklady*, vol. **262**, pp. 71–75.

Brini, F. & Ruggeri, T. 2020 Second-order approximation of extended thermodynamics of a monatomic gas and hyperbolicity region. *Contin. Mech. Thermodyn.* **32** (1), 23–39.

Burnett, D. 1936 The distribution of molecular velocities and the mean motion in a non-uniform gas. *Proc. Lond. Math. Soc.* **2** (1), 382–435.

Cercignani, C. 1975 *Theory and Application of the Boltzmann Equation*. Scottish Academic Press.

Chapman, S. 1916 Vi. on the law of distribution of molecular velocities, and on the theory of viscosity and thermal conduction, in a non-uniform simple monatomic gas. *Phil. Trans. R. Soc. Lond. A* **216** (538–548), 279–348.

Chapman, S. & Cowling, T.G. 1970 *The Mathematical Theory of Non-Uniform Gases: An Account of the Kinetic Theory of Viscosity, Thermal Conduction and Diffusion in Gases*. Univ. Press.

Dreyer, W. 1987 Maximisation of the entropy in non-equilibrium. *J. Phys. A: Math. Gen.* **20** (18), 6505.

Enskog, D. 1917 *Kinetische Theorie der Vorgänge in mässig Verdünnten Gasen. I. Allgemeiner Teil*, vol. 1. Almquist & Wiksell.

García-Colín, L.S., Velasco, R.M. & Uribe, F.J. 2008 Beyond the Navier–Stokes equations: Burnett hydrodynamics. *Phys. Rep.* **465** (4), 149–189.

Grad, H. 1949 On the kinetic theory of rarefied gases. *Commun. Pure Appl. Maths* **2** (4), 331–407.

Grad, H. 1952 The profile of a steady plane shock wave. *Commun. Pure Appl. Maths* **5** (3), 257–300.

Grad, H. 1958 Principles of the kinetic theory of gases. In *Thermodynamik der Gase/Thermodynamics of Gases*, pp. 205–294. Springer.

Gu, X.-J. & Emerson, D.R. 2009 A high-order moment approach for capturing non-equilibrium phenomena in the transition regime. *J. Fluid Mech.* **636**, 177–216.

Guo, Y., Jou, D. & Wang, M. 2016 Understanding of flux-limited behaviors of heat transport in nonlinear regime. *Phys. Lett. A* **380** (3), 452–457.

Guyer, R.A. & Krumhansl, J.A. 1966 Thermal conductivity, second sound, and phonon hydrodynamic phenomena in nonmetallic crystals. *Phys. Rev.* **148** (2), 778.

Jadhav, R.S. & Agrawal, A. 2020*a* Grad's second problem and its solution within the framework of Burnett hydrodynamics. *J. Heat Transfer* **142** (10), 102105.

Jadhav, R.S. & Agrawal, A. 2020*b* Strong shock as a stringent test for Onsager–Burnett equations. *Phys. Rev. E* **102** (6), 063111.

Jadhav, R.S. & Agrawal, A. 2021*a* Evaluation of Grad's second problem using different higher order continuum theories. *J. Heat Transfer* **143** (1), 012102.

Jadhav, R.S. & Agrawal, A. 2021*b* Shock structures using the OBurnett equations in combination with the holian conjecture. *Fluids* **6** (12), 427.

JADHAV, R.S., GAVASANE, A. & AGRAWAL, A. 2021 Improved theory for shock waves using the OBurnett equations. *J. Fluid Mech.* **929**, A37.

JADHAV, R.S., SINGH, N. & AGRAWAL, A. 2017 Force-driven compressible plane Poiseuille flow by Onsager–Burnett equations. *Phys. Fluids* **29** (10), 102002.

JADHAV, R.S., YADAV, U. & AGRAWAL, A. 2023 OBurnett equations: thermodynamically consistent continuum theory beyond the Navier–Stokes regime. *ASME J. Heat Mass Transfer* **145** (6), 060801.

JIN, S. & SLEMROD, M. 2001 Regularization of the Burnett equations via relaxation. *J. Stat. Phys.* **103**, 1009–1033.

KOGAN, M.N. 1969 *Rarefied Gas Dynamics*. Springer.

MAHENDRA, A.K. & SINGH, R.K. 2013 Onsager reciprocity principle for kinetic models and kinetic schemes. arXiv preprint arXiv:1308.4119.

MANSOUR, M.M., BARAS, F. & GARCIA, A.L. 1997 On the validity of hydrodynamics in plane Poiseuille flows. *Physica A: Stat. Mech. Applics.* **240** (1-2), 255–267.

MCDONALD, J. & TORRILHON, M. 2013 Affordable robust moment closures for CFD based on the maximum-entropy hierarchy. *J. Comput. Phys.* **251**, 500–523.

MCDONALD, J.G. 2011 *Extended Fluid-Dynamic Modelling for Numerical Solution of Micro-Scale Flows*. University of Toronto.

MCDONALD, J.G. & GROTH, C.P.T. 2013 Towards realizable hyperbolic moment closures for viscous heat-conducting gas flows based on a maximum-entropy distribution. *Contin. Mech. Thermodyn.* **25**, 573–603.

MCLENNAN, J.A. 1974 Onsager's theorem and higher-order hydrodynamic equations. *Phys. Rev. A* **10** (4), 1272.

MÜLLER, I. & RUGGERI, T. 1993 Extended thermodynamics. In *Springer Tracts in Natural Philosophy*, vol. 37. Springer.

MYONG, R.S. 2011 A full analytical solution for the force-driven compressible Poiseuille gas flow based on a nonlinear coupled constitutive relation. *Phys. Fluids* **23** (1), 012002.

ONSAGER, L. 1931*a* Reciprocal relations in irreversible processes. I. *Phys. Rev.* **37** (4), 405.

ONSAGER, L. 1931*b* Reciprocal relations in irreversible processes. II. *Phys. Rev.* **38** (12), 2265.

ÖTTINGER, H.C. 2005 *Beyond Equilibrium Thermodynamics*. vol. **5**. Wiley-Interscience Hoboken.

ÖTTINGER, H.C. 2010 Thermodynamically admissible 13 moment equations from the Boltzmann equation. *Phys. Rev. Lett.* **104** (12), 120601.

RANA, A., RAVICHANDRAN, R., PARK, J.H. & MYONG, R.S. 2016 Microscopic molecular dynamics characterization of the second-order non-Navier–Fourier constitutive laws in the Poiseuille gas flow. *Phys. Fluids* **28** (8), 082003.

RANA, A.S., GUPTA, V.K., SPRITTLES, J.E. & TORRILHON, M. 2021 H-theorem and boundary conditions for the linear R26 equations: application to flow past an evaporating droplet. *J. Fluid Mech.* **924**, A16.

RANA, A.S., GUPTA, V.K. & STRUCHTRUP, H. 2018 Coupled constitutive relations: a second law based higher-order closure for hydrodynamics. *Proc. R. Soc. A: Math. Phys. Engng Sci.* **474** (2218), 20180323.

RANA, A.S. & STRUCHTRUP, H. 2016 Thermodynamically admissible boundary conditions for the regularized 13 moment equations. *Phys. Fluids* **28** (2), 027105.

REITEBUCH, D. & WEISS, W. 1999 Application of high moment theory to the plane Couette flow. *Contin. Mech. Thermodyn.* **11** (4), 217–225.

ROMERO, M.B. & VELASCO, R.M. 1995 Onsager's symmetry in the Burnett regime. *Physica A: Stat. Mech. Applics.* **222** (1-4), 161–172.

SHAVALIYEV, M.S. 1993 Super-Burnett corrections to the stress tensor and the heat flux in a gas of Maxwellian molecules. *J. Appl. Maths Mech.* **57** (3), 573–576.

SINGH, N. & AGRAWAL, A. 2016 Onsager's-principle-consistent 13-moment transport equations. *Phys. Rev. E* **93** (6), 063111.

SINGH, N., JADHAV, R.S. & AGRAWAL, A. 2017 Derivation of stable Burnett equations for rarefied gas flows. *Phys. Rev. E* **96** (1), 013106.

SONE, Y. 2000 Flows induced by temperature fields in a rarefied gas and their ghost effect on the behavior of a gas in the continuum limit. *Annu. Rev. Fluid Mech.* **32** (1), 779–811.

STRUCHTRUP, H. 2004 Stable transport equations for rarefied gases at high orders in the Knudsen number. *Phys. Fluids* **16** (11), 3921–3934.

STRUCHTRUP, H. 2005 *Macroscopic Transport Equations for Rarefied Gas Flows: Approximation Methods in Kinetic Theory*, 1st edn. Springer.

STRUCHTRUP, H. & TORRILHON, M. 2003 Regularization of Grad's 13 moment equations: derivation and linear analysis. *Phys. Fluids* **15** (9), 2668–2680.

STRUCHTRUP, H. & TORRILHON, M. 2007 H theorem, regularization, and boundary conditions for linearized 13 moment equations. *Phys. Rev. Lett.* **99** (1), 014502.

TAHERI, P., TORRILHON, M. & STRUCHTRUP, H. 2009 Couette and Poiseuille microflows: analytical solutions for regularized 13-moment equations. *Phys. Fluids* **21** (1), 017102.
TIBBS, K.W., BARAS, F. & GARCIA, A.L. 1997 Anomalous flow profile due to the curvature effect on slip length. *Phys. Rev. E* **56** (2), 2282.
TIJ, M. & SANTOS, A. 1994 Perturbation analysis of a stationary nonequilibrium flow generated by an external force. *J. Stat. Phys.* **76**, 1399–1414.
TIMOKHIN, M.Y., STRUCHTRUP, H., KOKHANCHIK, A.A. & BONDAR, Y.A. 2017 Different variants of R13 moment equations applied to the shock-wave structure. *Phys. Fluids* **29** (3), 037105.
TODD, B.D. & EVANS, D.J. 1997 Temperature profile for Poiseuille flow. *Phys. Rev. E* **55** (3), 2800.
TORRILHON, M. 2016 Modeling nonequilibrium gas flow based on moment equations. *Annu. Rev. Fluid Mech.* **48**, 429–458.
TORRILHON, M. & STRUCHTRUP, H. 2004 Regularized 13-moment equations: shock structure calculations and comparison to Burnett models. *J. Fluid Mech.* **513**, 171–198.
TRUESDELL, C. & MUNCASTER, R.G. 1980 *Fundamentals of Maxwell's Kinetic Theory of a Simple Monatomic Gas: Treated as a Branch of Rational Mechanics*. Academic Press.
URIBE, F.J. & GARCIA, A.L. 1999 Burnett description for plane Poiseuille flow. *Phys. Rev. E* **60** (4), 4063.
WEISS, W. 1995 Continuous shock structure in extended thermodynamics. *Phys. Rev. E* **52** (6), R5760.
XU, K. 2003 Super-Burnett solutions for Poiseuille flow. *Phys. Fluids* **15** (7), 2077–2080.
YADAV, U. & AGRAWAL, A. 2021 Analysis of Burnett stresses and entropy generation for pressure-driven plane Poiseuille flow. *ASME. J. Heat Transfer* **143** (3), 032102.
YADAV, U. & AGRAWAL, A. 2024 Capturing non-equilibrium effects in cylindrical Couette flow problem using the extended Onsager-13 moment equations. *Phys. Fluids* **36** (1), 012007.
YADAV, U., JONNALAGADDA, A. & AGRAWAL, A. 2023 Third-order accurate 13-moment equations for non-continuum transport phenomenon. *AIP Adv.* **13** (4), 045311.
YADAV, U., JONNALAGADDA, A. & AGRAWAL, A. 2024 Derivation of extended-OBurnett and super-OBurnett equations and their analytical solution to plane Poiseuille flow at non-zero Knudsen number. *J. Fluid Mech.* **983**, A29.
ZHAO, W., CHEN, W. & AGARWAL, R.K. 2014 Formulation of a new set of simplified conventional Burnett equations for computation of rarefied hypersonic flows. *Aerosp. Sci. Technol.* **38**, 64–75.
ZHENG, Y., GARCIA, A.L. & ALDER, B.J. 2002 Comparison of kinetic theory and hydrodynamics for Poiseuille flow. *J. Stat. Phys.* **109** (3), 495–505.
ZHENG, Y., GARCIA, A.L. & ALDER, B.J. 2003 Comparison of kinetic theory and hydrodynamics for Poiseuille flow. In AIP Conference Proceedings, vol. **663**, pp. 149–156. American Institute of Physics.
ZHONG, X., MACCORMACK, R.W. & CHAPMAN, D.R. 1993 Stabilization of the Burnett equations and application to hypersonic flows. *AIAA J.* **31** (6), 1036–1043.
ZOHAR, Y., LEE, S.Y.K., LEE, W.Y., JIANG, L. & TONG, P. 2002 Subsonic gas flow in a straight and uniform microchannel. *J. Fluid Mech.* **472**, 125–151.